GeoExpert ag

swiss*nuclear*: PEGASOS Refinement Project:
SP2 – Ground Motion Characterization

Contract no. PMT-VT-1032

Seismic Shear Wave Velocity Determination and Hybrid Seismic Survey at the SED-Station WEIN (Weingarten TG)

Date of Field Data Acquisition 4th March 2009

Revised Report

Client

swiss*nuclear*
Project PRP
Frohburgstrasse 17
4601 Olten

Contractor

GeoExpert ag
Seismic Prospecting
Ifangstrasse 12b
P.O. Box 451
8603 Schwerzenbach

8603 Schwerzenbach, 13th May 2009

INDEX

1 INTRODUCTION

1.1 Survey objectives

The seismic survey's main task is to provide information about the distribution function of the shear wave velocities in the depth interval of the uppermost 30 m along a 100 m long seismic profile.

Additionally, the following objectives are to be met:

- the mapping of the topography of the rock face, i.e. the thickness of the Quaternary deposits;
- the determination of the thickness of the weathered zone and its degree of decompaction at the bedrock surface;
- a general view of geological structures.

1.2 The choice of the appropriate surveying methods

Several methods are available for deriving the s-wave velocity distribution in the subsurface at any given position:

- in-situ measurement by down-hole or crosshole seismic surveying;
- shear-wave refraction tomography profiling;
- dispersion analysis of surface waves (MASW; **M**ultiple channel **A**nalysis of **S**urface **W**aves)

The surveys are to be carried out at, or as close as possible near some 20 SED earth quake monitoring stations in Switzerland. Ideally, the surveys are to be conducted on two orthogonal profiles in order to derive at their point of intersection a robust 1D s-wave velocity distribution function by correlation. To this end, the methods of MASW and shear-wave refraction tomography profiling are to be combined.

The results are to include the following fundamental parameters $v_{s,5}$, $v_{s,10}$, $v_{s,20}$, $v_{s,30}$, $v_{s,40}$, $v_{s,50}$, $v_{s,100}$ are to be calculated, also an error estimation of all values.

The data acquired for the MASW method are to be subjected to complementary **p-wave hybrid seismic data processing** in order to image the geological structures.

2 FIELD DATA ACQUISITION PARTICULARS

2.1 Time Schedule

Date	*Time*	*Activities / remarks*
03.03.2009	0800	arrival from Klingnau
	0800 - 0830	site reconnaissance
	0830 - 1000	lay-out of recording spread profile 1 p- and s-wave
	1000 - 1040	compressional wave data recording line 1
	1115 - 1155	shear wave data recording line 1
	1330 - 1500	lay-out of recording spread profile 2 p- and s-wave
	1500 - 1530	compressional wave data recording line 2
	1600 - 1645	shear wave data recording line 2
	1645 - 1710	retrieval of the recording spread
	1715	departure from site

2.2 Summary of Data Acquisition Parameters

Compressional Wave Data Acquisition

# of active channels	96
geophone type	4.5 Hz natural frequency, vertical velocimeter
receiver station spacing	1.0 m
# of geophones/station	1
source point spacing	2.0 m to 3.0 m
source type	vertical hammer (6 kg) striking on a horizontal metal plate
sampling rate	500 µs
recording time	2048 ms
field filters	0.5 Hz LC, anti-alias
# of field records	47 (line 09SN_18WEIN-P1) and 48 (line 09SN_18WEIN-P2)

Shear Wave Data Acquisition

# of active channels	48
geophone type	10 Hz natural frequency, horizontal velocimeter
receiver station spacing	2.0 m
# of geophones/station	1
source point spacing	4.0 m to 6.0 m
source type	horizontal hammer (6 kg) striking horizontally at a metal-plated wooden beam anchored to the ground by means of 20 cm long spikes
sampling rate	500 µs
recording time	1024 ms
field filters	2 Hz LC, anti-alias
# of field records	30 at 15 positions on both lines 09SN_18WEIN-S1 and 09SN_18WEIN-S2

Fig. 2.1: S-wave data acquisition at profile 1.

2.3 Composition of Seismic Field Crew

Personnel

Jochen Fiseli	Dipl.-Geolog, University of Freiburg I. Br., party chief
Dieter Martin	Dipl.-Geolog, University of Freiburg I. Br., party chief
Kieron Lynch	assistant, spread lay-out and activation of seismic source
Fabian Isler	assistant, spread lay-out and activation of seismic source

Equipment

96	vertical geophones 4.5 Hz
48	horizontal geophones 12 Hz
6	seismic cables
1	seismic acquisition system Summit Compact, 96 channels
1	laptop computer for data acquisition
3	walkie-talkies
1	hammer 6 kg
1	steel plate
1	metal-plated wooden beam
1	van (FIAT Ducato 4x4)

2.4 Location

The seismic monitoring station WEIN (Weingarten TG) is situated on a slope of a molasse sediment ridge (clastic Upper Freshwater Molasse, mainly Nagelfluh) in northeastern Switzerland, canton of Thurgau, immediatly adjacent to Quaternary slope wash and alluvial fan deposits. The Tertiary sediments are covered with glacial till.

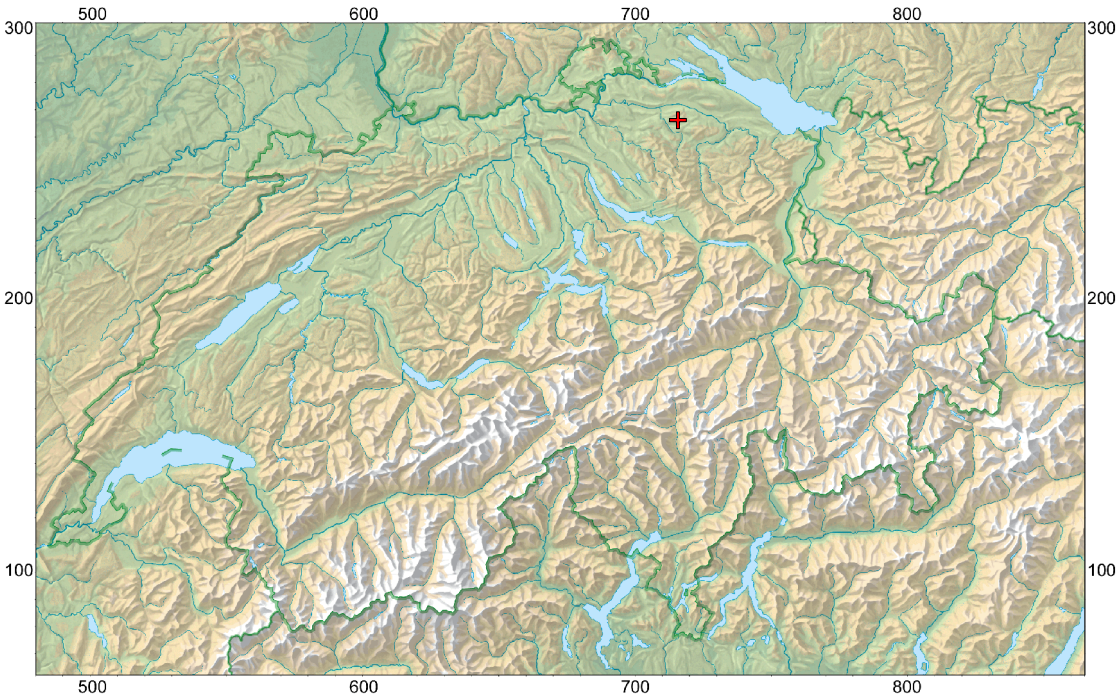

Fig. 2.2: The red cross marked seismic monitoring station WEIN (Weingarten TG) located in Thurgau's Tertiary sediments (Upper Freshwater Molasse). (map: geodata @ swisstopo).

2.5 Recording Conditions and Line Setup

Drizzle and low temperatures prevailed throughout the field data recording period. The environment is calm and no electromagnetic interferences are observed.

In general, the seismic data quality obtained at WEIN is to be rated as good with a high surface-wave content.

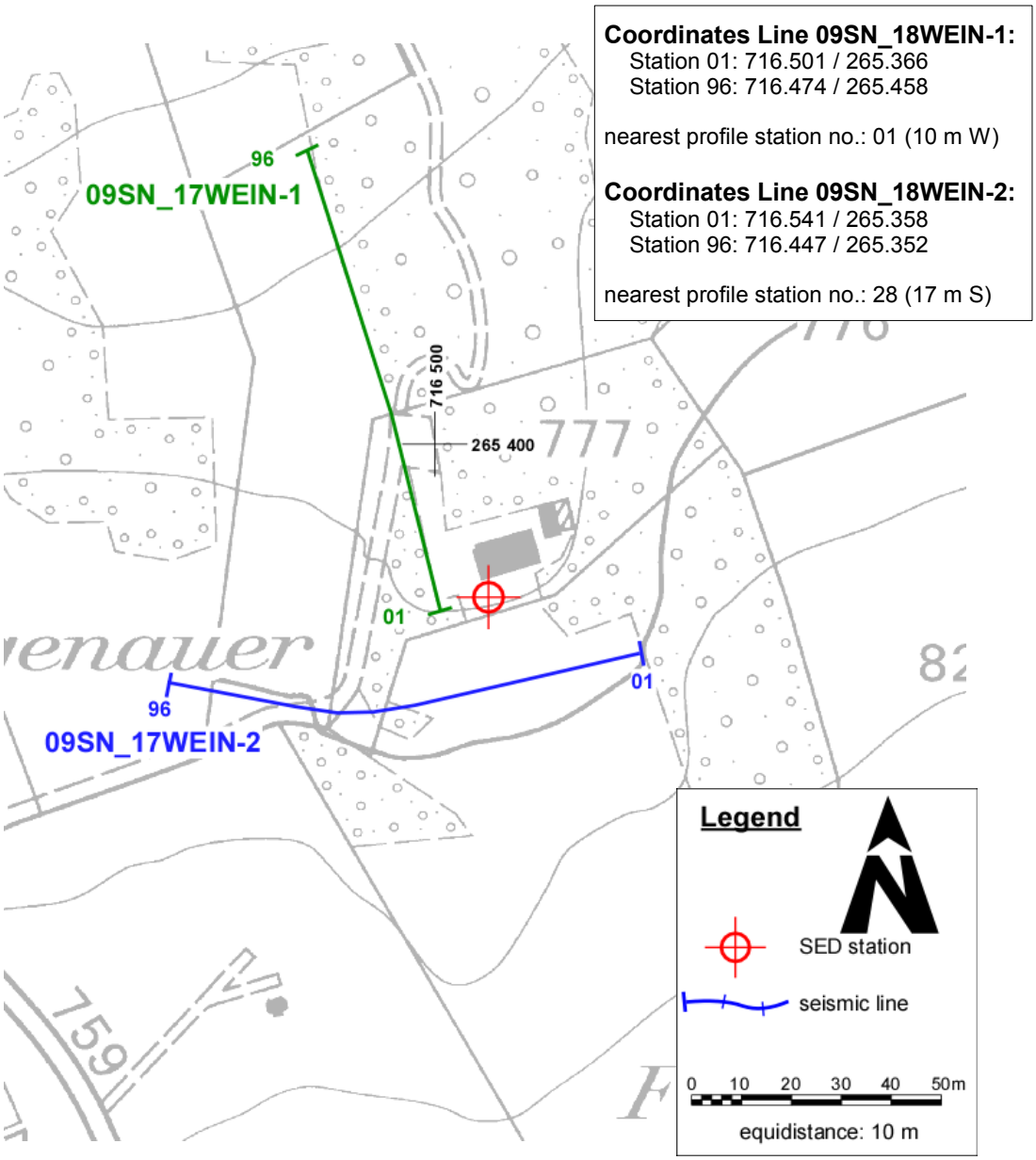

Fig. 2.3: Situation map with the trace of seismic profile 09SN_18WEIN-1 and -2. (background map: © 2006 Amt für Geoinformation Kanton Thurgau)

3 SEISMIC DATA PROCESSING AND IMAGING OF THE RESULTS

3.1 General Remarks

- For the shear and compressional wave refraction seismic evaluation the package **RAYFRACT** by Intelligent Resources Ltd., Vancouver CAN, was used. The system features the technique of diving wave tomography (www.rayfract.com).
- The system **SPW** (**S**eismic **P**rocessing **W**orkshop) of Parallel Geoscience Corporation, Austin US-TX, was used for reflection seismic data processing (www.parallelgeo.com).
- Data processing of surface waves (MASW processing) was conducted with the software package **SurfSeis** V2.0 of Kansas Geological Survey in Lawrence US-KS.

A detailed description of the various surveying methods will be included in the general summary report.

3.2 Shear Wave Refraction Tomography

3.2.1 Reformatting and field geometry assignment

After reformatting the field data into the Rayfract format the field geometry is applied.

3.2.2 First break time picking

At each shot position, two seismic records were acquired in both activation directions. These two records are displayed superimposed with different colors on each other in Fig 3.2a together with the manually determined first arrival time picks.

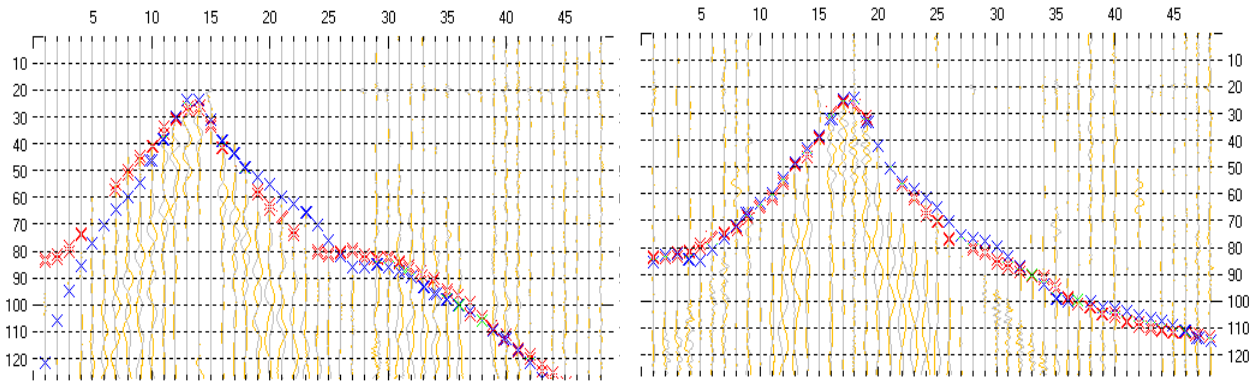

*Fig. 3.2a: High quality dual field record from line 09SN_18WEIN-S1 (left) and 09SN_18WEIN-S2 (right).showing at each station the s-wave traces with opposing polarities in different colors. The manually picked s-wave refraction arrivals at each station are marked with an **x**. Marks in blue (**x**) shows the raytraced first break travel time picks after iteration. The station spacing is 2 m, profile station number 0 = profile meter 0; profile station number 48 = profile meter 96.*

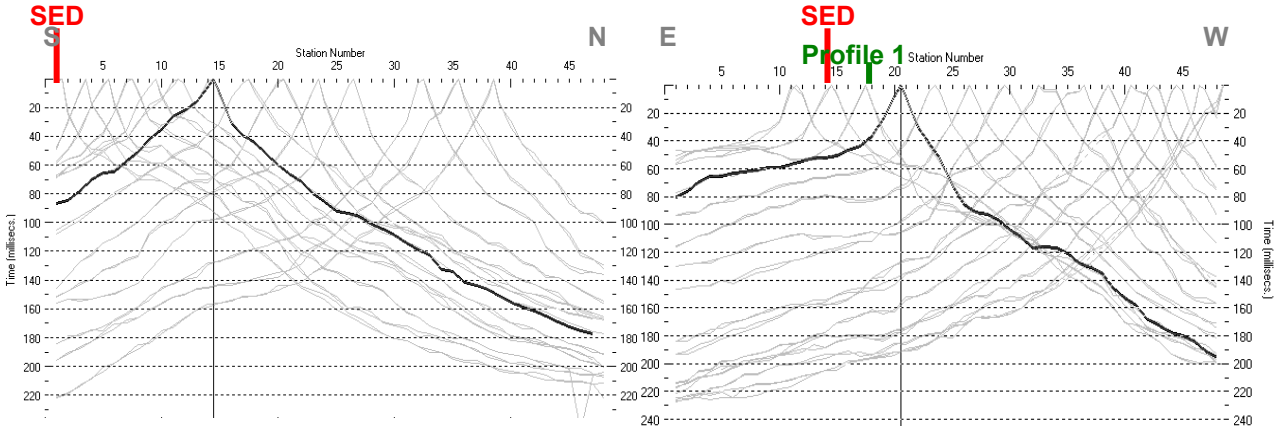

Fig. 3.2b: Curves of s-wave first break time picks from line 09SN_18WEIN-S1 (left) and 09SN_18-WEIN-S2 (right).

3.2.3 Analytical Determination of Refraction Velocities

An initial 1D-velocity function (averaged 1D velocity-depth profiles derived by the Delta-t-V method, see Tab. 3.2a) is determined in the 3-dimensional time-offset-CMP-domain from all first break arrival time curves in the 3-dimensional time-offset-CMP-domain (see. Fig. 3.2c).

Depth [m]	Vs [m/s]
0.0	192
0.6	194
0.9	213
1.5	241
2.2	282
3.5	350
5.0	388
7.2	416
10.3	472
14.8	573
20.9	677
29.3	950
41.3	1671

Depth [m]	Vs [m/s]
0.0	137
0.5	145
0.9	154
1.4	158
2.1	175
3.4	248
4.8	378
6.9	613
9.9	784
14.2	592
20.1	509
28.2	710
39.8	1160

Tab. 3.2a: Initial 1D s-wave velocity function derived from real data from line 09SN_18WEIN-S1 (mean values between profile meters 30 and 50) and from line 09SN_18WEIN-S2 (mean values between profile meters 5 and 45).

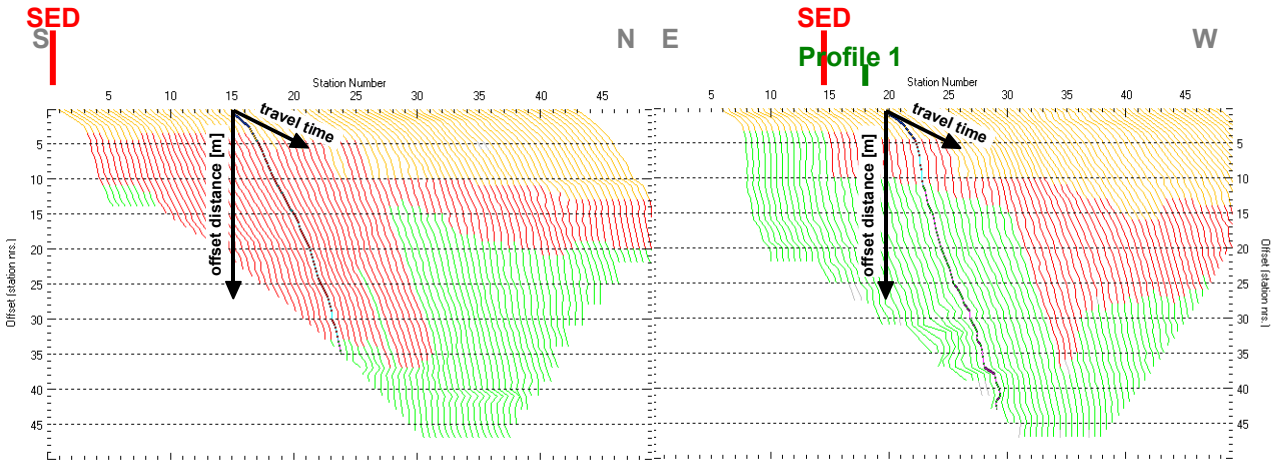

Fig. 3.2c: 3-dimensional distance-travel time diagrams from line 09SN_18WEIN-S1 (left) and 09SN_18-WEIN-S2 (right) at the mid-points between source points and receiver stations are instrumental when using the analytical CMP derivation of the initial velocity field.
The horizontal axes are the along the CMP positions and the travel time respectively, the vertical axis denotes the offset distance between source and receiver positions. The colors represent different velocity layers. The station spacing is 2 m, profile station number 00 = profile meter 0; profile station number 48 = profile meter 96. The colors represent different velocity layers.

3.2.4 Tomographic inversion of the velocity gradient field by iterative modeling

The velocity field is iteratively refined by the subsequent Wavepath Eikonal Traveltime (WET) tomographic inversion process. The inversion results are portrayed in Fig. 3.2d as a gridded velocity contour section and in Fig. 3.2e as a ray path density section.

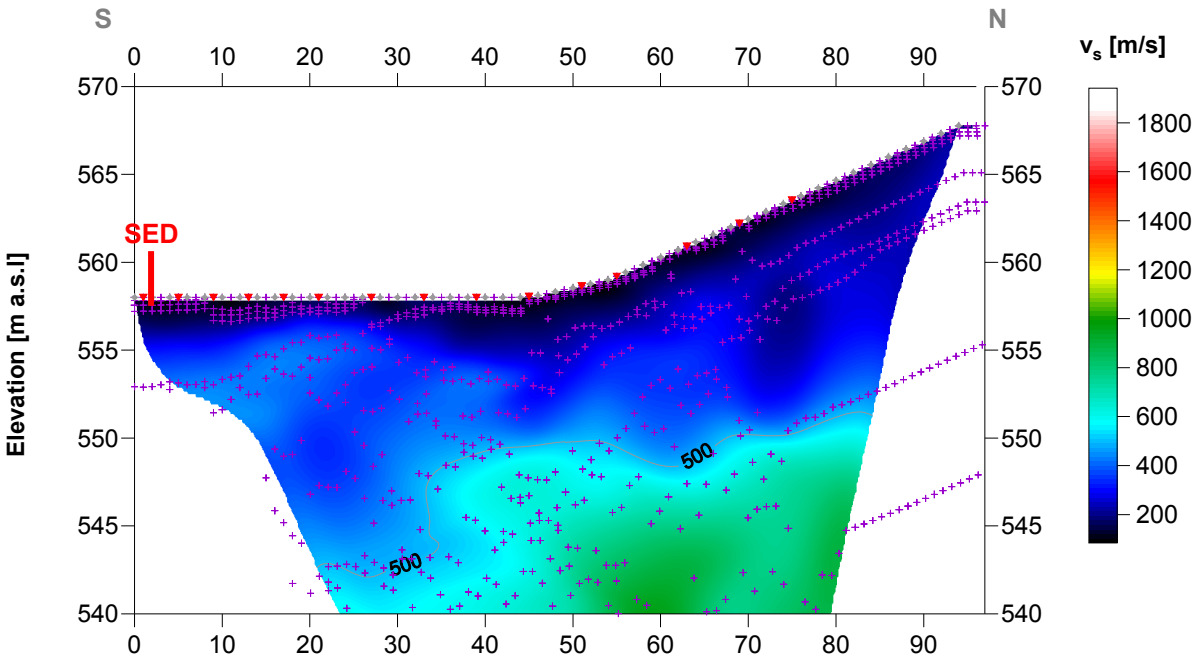

Fig. 3.2d: Shear wave velocity field of the line 09SN_18WEIN-S1. Red/white colors denote solid rock, blue/black colors point to unconsolidated sediments and soil.
Vertical axis: elevation [m a.s.l]; horizontal axis: profile meter; color encoded scale: v_s [m/s]; vertical exaggeration: 2:1; gray diamonds: receiver positions; red triangles: source positions; magenta crosses: positions of determined velocity values. The station spacing is 2 m, profile meter 0 = profile station number 0, profile meter 96 = profile station number 48.

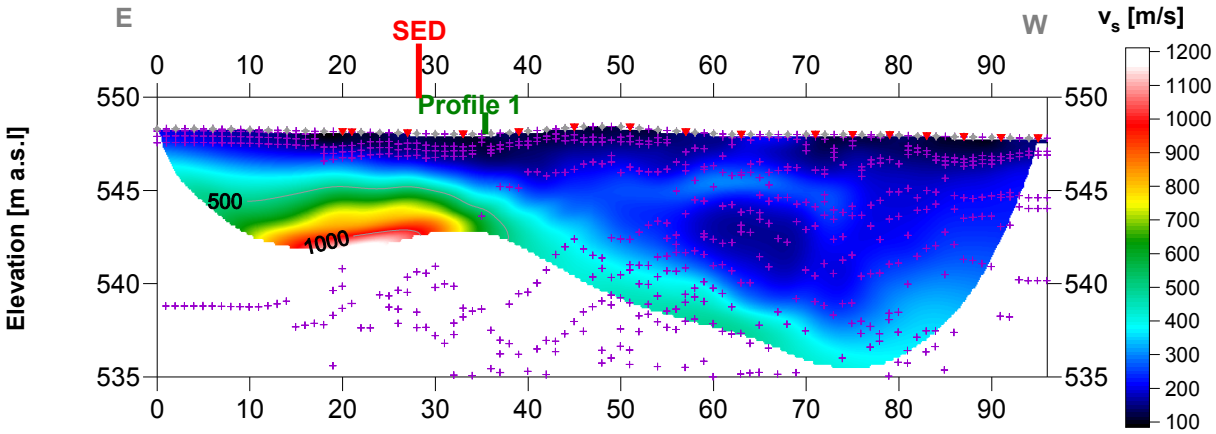

Fig. 3.2e: Shear wave velocity field of the line 09SN_18WEIN-S2. Red/white colors denote solid rock, blue/black colors point to unconsolidated sediments and soil.
Vertical axis: elevation [m a.s.l]; horizontal axis: profile meter; color encoded scale: v_s [m/s]; vertical exaggeration: 2:1; gray diamonds: receiver positions; red triangles: source positions; magenta crosses: positions of determined velocity values. The station spacing is 2 m, profile meter 0 = profile station number 00, profile meter 96 = profile station number 48.

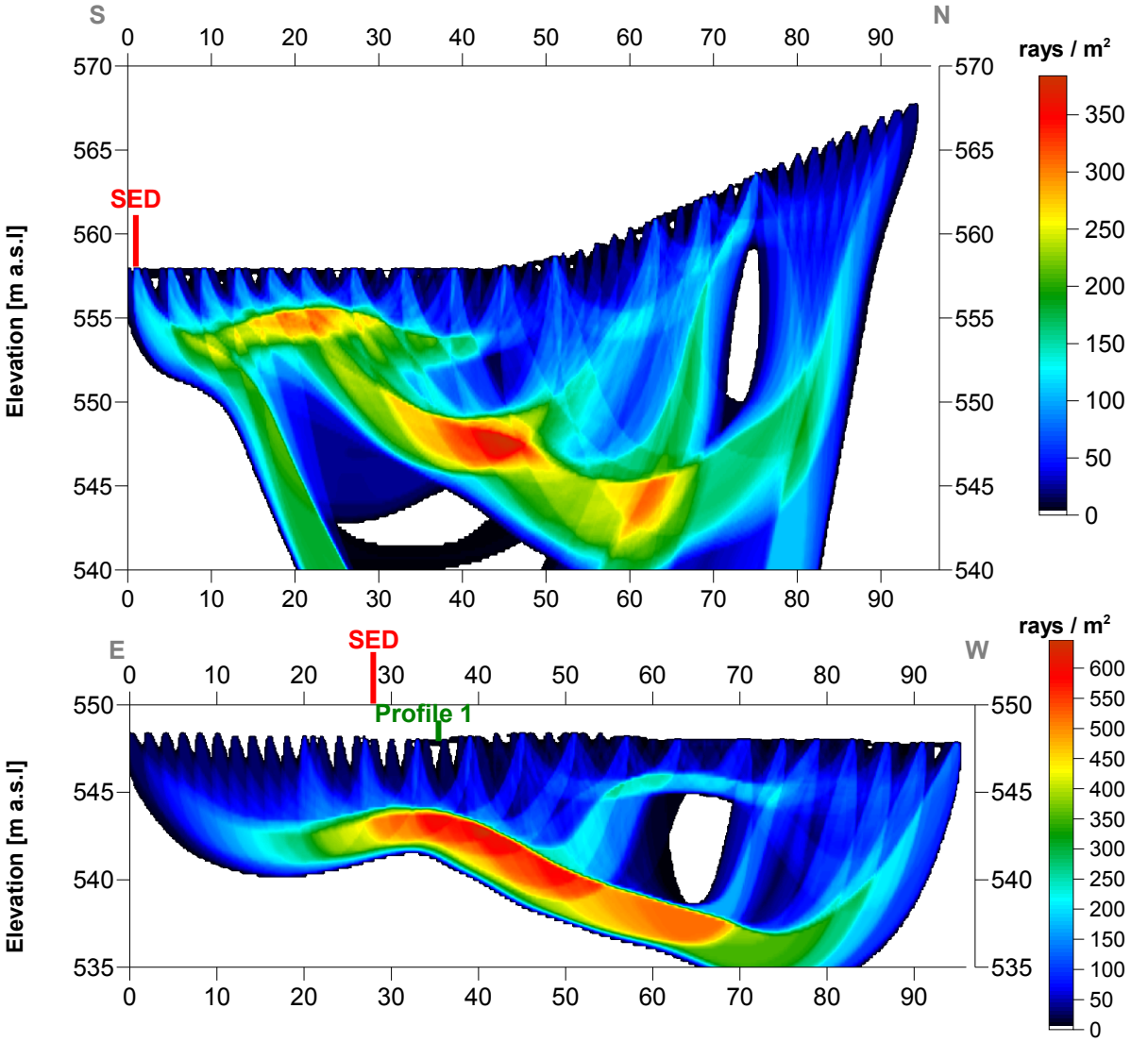

Fig. 3.2f: Shear wave ray path density along the seismic line 09SN_18WEIN-S1 (top) and -S2 (bottom). Red/white colors indicate high velocity contrasts (usually at the bedrock surface), blue/black colors denote low coverage areas. Vertical axis: elevation [m a.s.l]; horizontal axis: profile meter; color encoded scale: ray paths per m²; vertical exaggeration: 2:1. The station spacing is 2 m, profile meter 0 = profile station 00, profile meter 96 = profile station 48.

Depth [m]	Vs [m/s]
0.0	139
1.7	246
3.3	355
5.0	395
6.6	392
8.3	415
10.0	459
11.6	483
13.3	495
14.9	517
16.4	567
18.1	609
19.7	649
21.4	689
23.1	762
24.7	837
26.4	923
28.1	1039
29.7	1164

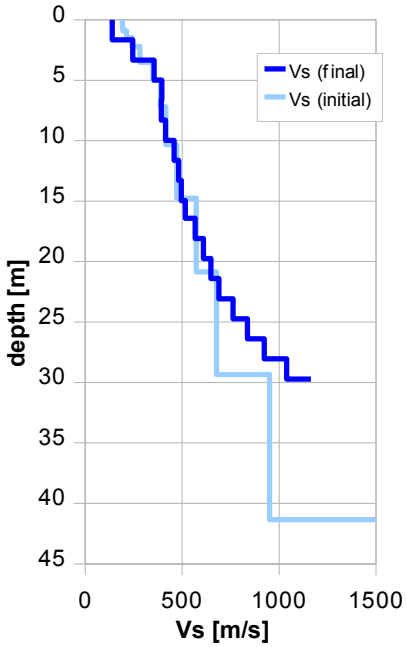

Tab. 3.2b: Final 1D s-wave velocity model derived from real data from line 09SN_18WEIN-S1 (horizontal average of all values) for the profile segment (between profile meters 5 and 45) with a geological setting resembling the one at the SED station. The calculated values of the initial 1D s-wave velocity model are given in Tab. 3.2a.

Depth [m]	Vs [m/s]
0.0	117
0.7	134
1.4	169
2.1	230
2.8	308
3.6	386
4.3	458
5.0	516
5.7	379
6.4	384
7.1	390
7.8	408
8.5	432
9.2	448

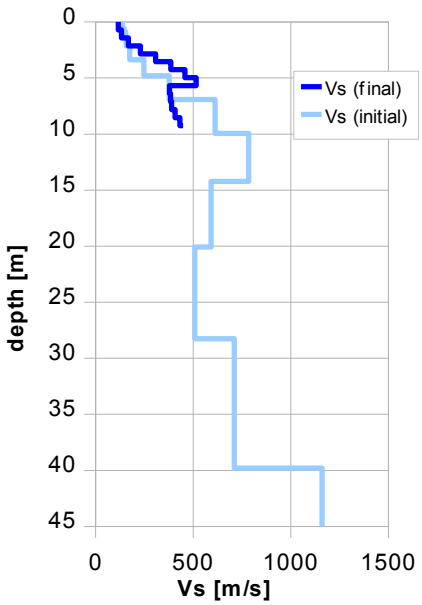

Tab. 3.2c: Final 1D s-wave velocity model derived from real data from line 09SN_18WEIN-S2 (horizontal average of all values) for the profile segment (between profile meters 30 and 50) with a geological setting resembling the one at the SED station. The calculated values of the initial 1D s-wave velocity model are given in Tab. 3.2a.

The attained depth of investigation being limited to 9 m on line 09SN_18WEIN-S1 is to be attributed to the method inherent constraining factor of critically refracted waves along the shallow bedrock surface (hard-kick), combined with the insufficient length of the lay-out spread for recording long offset data needed for deeper penetration.

3.3 MASW Processing

3.3.1 Reformatting and field geometry assignment

The data preparation steps for the dispersion analysis include

- the assignment of the field acquisition geometry
- the selection of suitable offset ranges (=arrays) between 10 m and 50 m for dispersion, and the splitting of the field records in forward and reverse shooting direction data sets
- the reformatting of the data into the specific KGS format

X - - ... - - o-o-o-...-o-o-o (forward shooting or so-called PLUS direction)
respectively
o-o-o-...-o-o-o - - ... - - X (reverse shooting or so-called MINUS direction).

where **X** = shot position
o = receiver station
- = 1.0 m offset

The active array used at SED-station WEIN are the receiver station in the shot offset range between 10 and 50 m.

3.3.2 Calculating the dispersion image (overtone)

The result of dispersion analysis is the color encoded acoustic energy distribution in the phase velocity - frequency plane (see Fig. 3.3a and b).

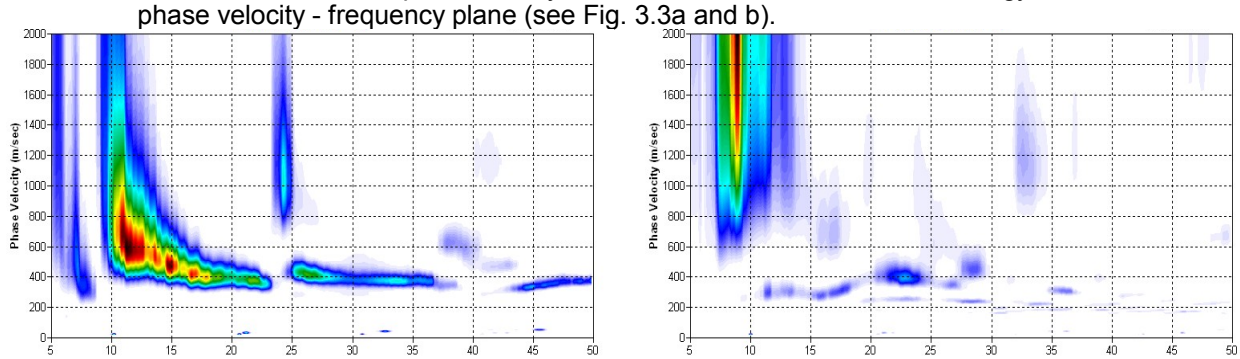

Fig. 3.3a: Dispersion image of fair to high quality data (left) from midpoint station 79 as found on 66 % and of deficient quality data (right) from midpoint station 33 representing about 33 % of the MASW dataset of site WEIN.
Horizontal axis: frequency from 5 to 50 Hz; vertical axis: phase velocity from 0 to 2000 m/s; color code: colors from white (no energy) to blue - green - yellow - red - black point to increasing energy amplitude values.

3.3.3 Analysis of the dispersion image

In the dispersion graphs as calculated in section 3.3.2 above, the curves joining the amplitude peaks of the fundamental modes are determined either by subjective inspection or in a semi-automated manner. On datasets with poorly defined amplitude peaks or with a highly irregular alignment of the peaks, the danger of obtaining improbable or wrong results is real and can only be mitigated by the processing experience and the a-priori knowledge of the geological setting by the geophysicist responsible for the data evaluation.

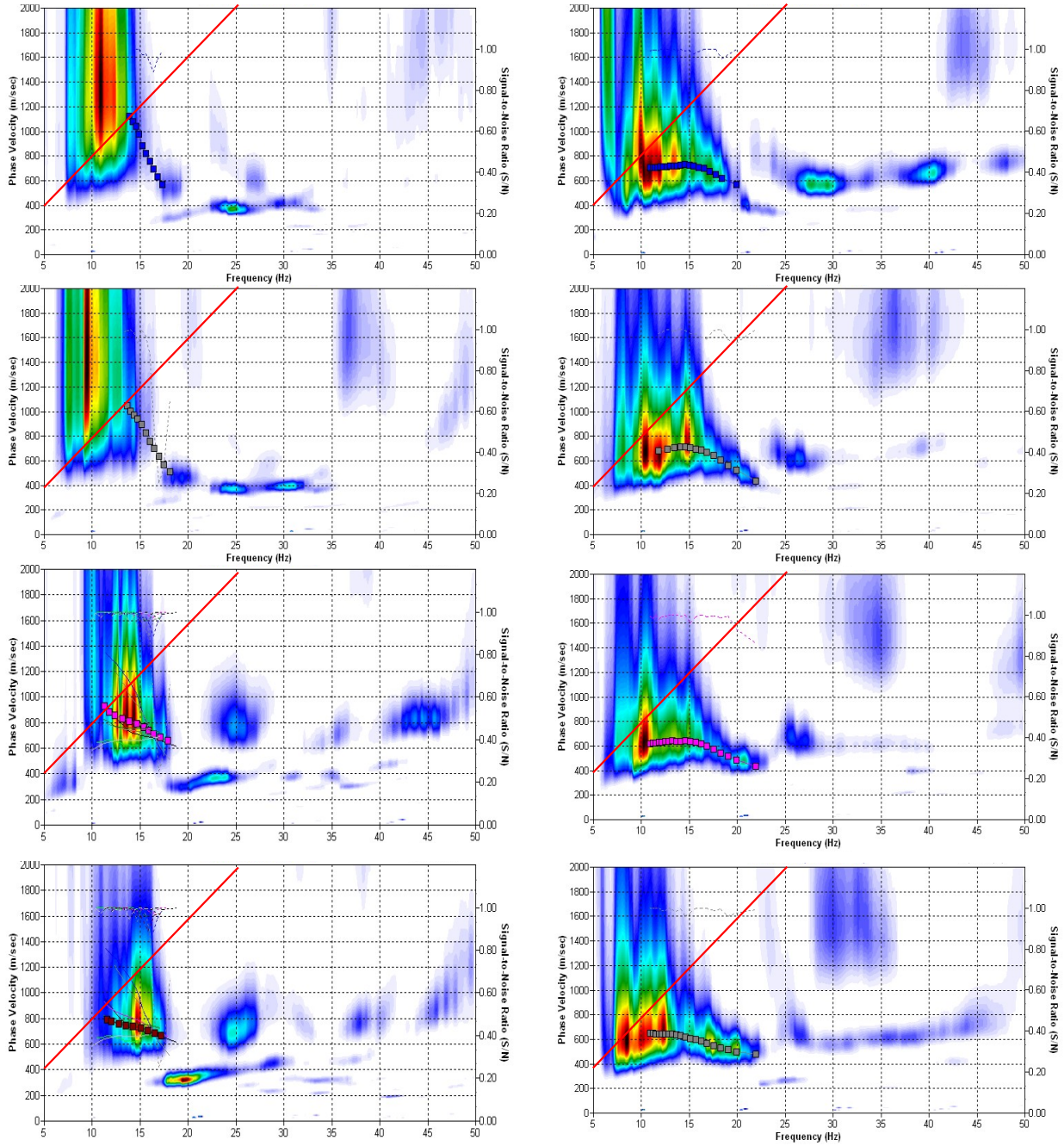

Fig. 3.3b: The manually picked dispersion images used for the derivation of the shear wave velocity section on line 09SN_18WEIN-M1. The dispersion curves (squares) are determined by linking the peaks of high energy. Note that 'higher modes' may at times produce higher energy peaks than the fundamental mode required for the analysis.
dotted fine line: signal-noise ratio for the designated f-v_{ph} – value.
red line: high resolution beam-forming curve for v_{max}.
1st row: left: station 35 @ PLUS direction; right: station 37 @ MINUS direction
2nd row: left: station 38 @ PLUS direction; right: station 40 @ MINUS direction
3rd row: left: station 47 @ PLUS direction; right: station 43 @ MINUS direction
4th row: left: station 50 @ PLUS direction; right: station 46 @ MINUS direction

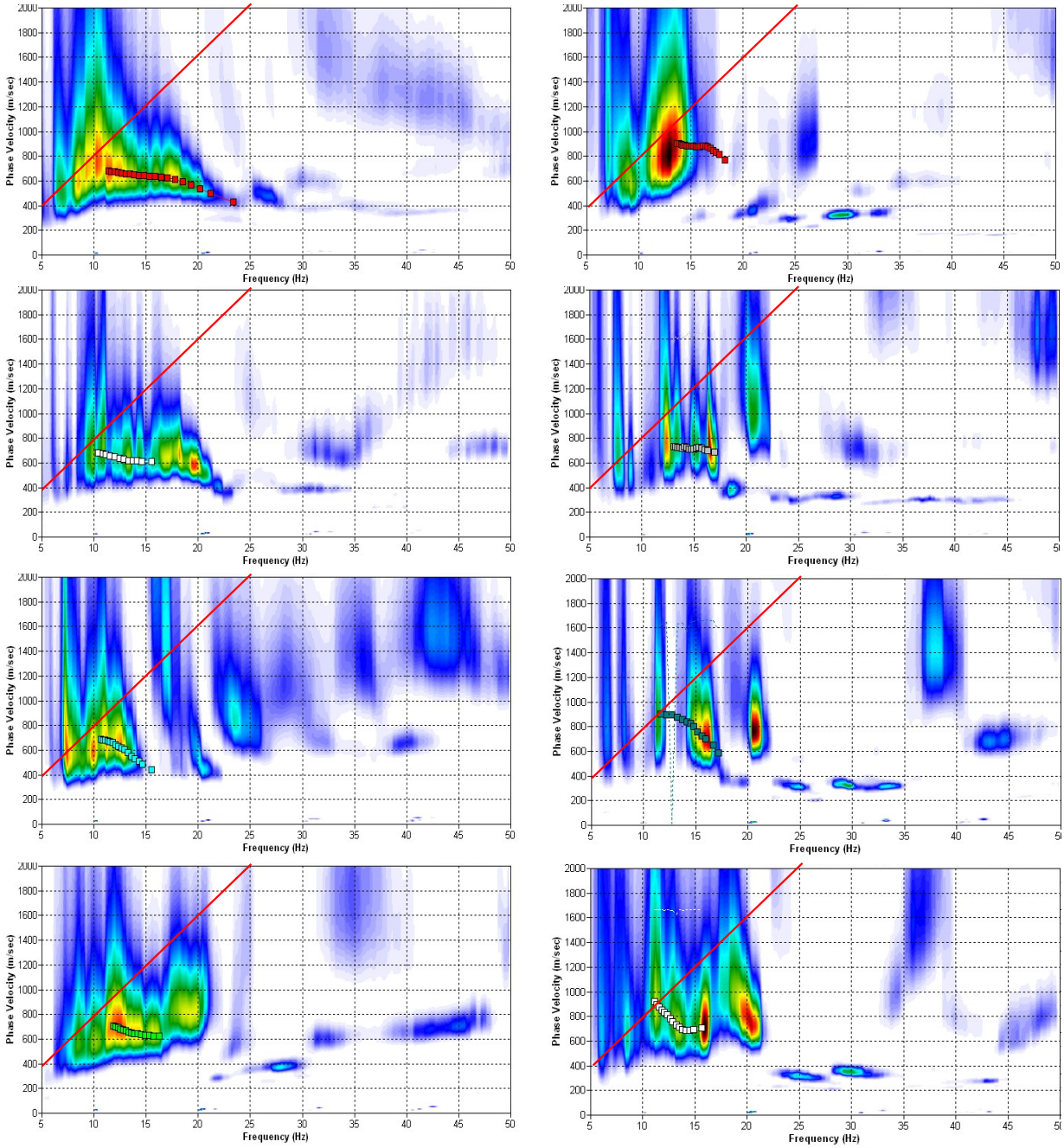

Fig. 3.3c: The manually picked dispersion images used for the derivation of the shear wave velocity section on line 09SN_18WEIN-M2. The dispersion curves (squares) are determined by linking the peaks of high energy. Note that 'higher modes' may at times produce higher energy peaks than the fundamental mode required for the analysis.
dotted fine line: signal-noise ratio for the designated f-v_{ph} – value.
red line: high resolution beam-forming curve for v_{max}.
1st row: left: station 31 @ PLUS direction; right: station 31 @ MINUS direction
2nd row: left: station 37 @ PLUS direction; right: station 40 @ MINUS direction
3rd row: left: station 41 @ PLUS direction; right: station 46 @ MINUS direction
4th row: left: station 47 @ PLUS direction; right: station 49 @ MINUS direction

3.3.4 Inversion of dispersion curves resulting in a 1D shear wave velocity distribution

Inversion of the extracted dispersion curves was performed using the algorithm described by Xia et al. (1999).

The inversion process is started by setting the maximum depth (z_{max}) to be in the order of 30% of the largest wavelength for an initial model consisting of 10 layers of increasing thicknesses. For all 10 layers the Poisson's ratio is assumed to be 0.4 and the rock/soil density to be 2.0 g/cm^3. The inversion process is concluded either after twelve iterations or when the convergence condition of a RMS-error of less than 3 m/s (phase velocity) is met.

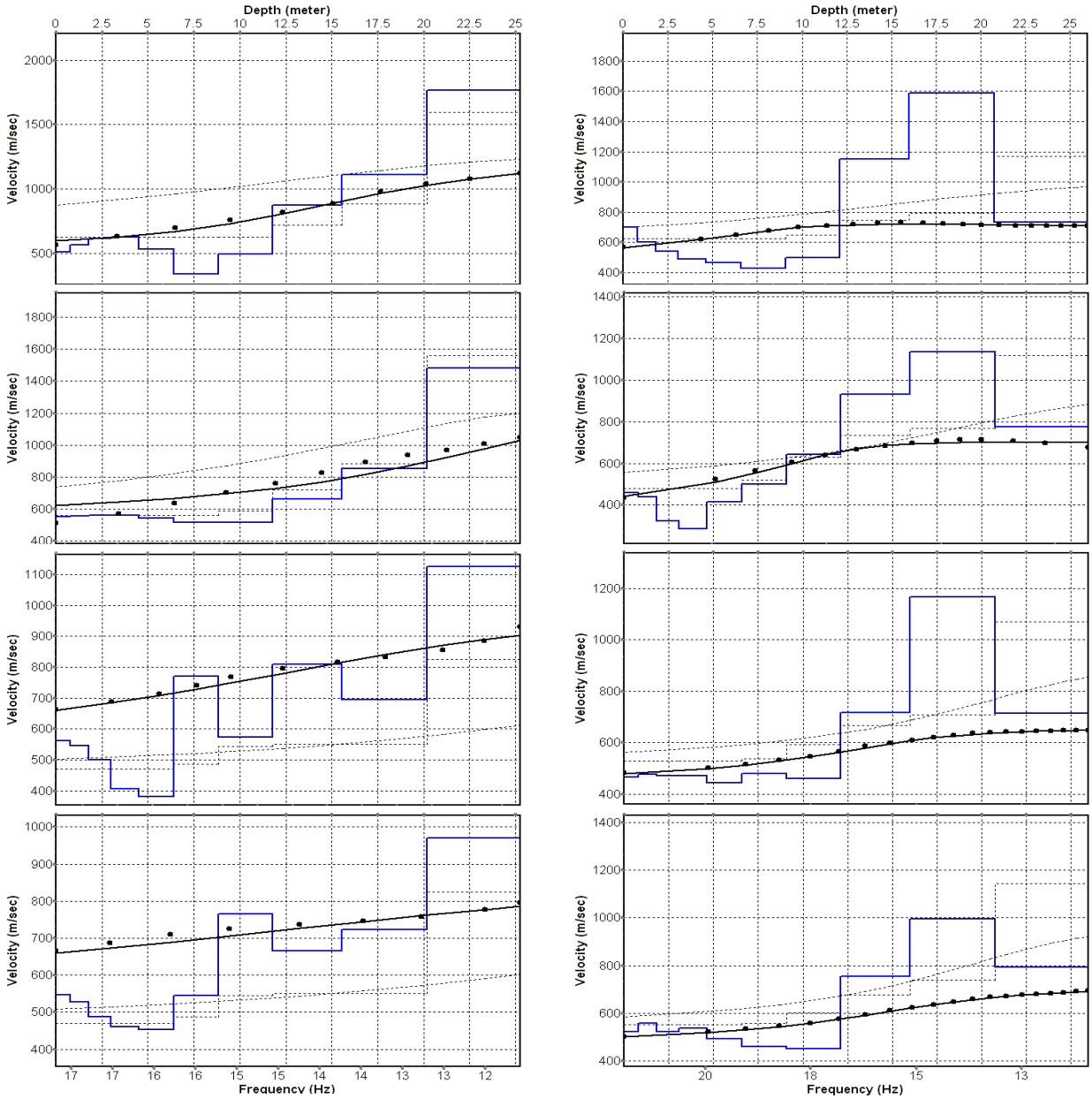

Fig. 3.3d: Inversion results of dispersion curves from dataset at line 09SN_18WEIN-M1.
***brown**: Inversion of dispersion curve (dots) resp. of the modeled dispersion curve (dotted line: initial model; continuous line: end model). Horizontal axis: frequency Hz, vertical axis: v_s.*
***blue**: 10-layer-model (dotted: initial model, continuous line: final model). Horizontal axis: depth, vertical axis: phase velocity resp. v_s).*
1st row: left: station 35 @ PLUS direction; right: station 37 @ MINUS direction
2nd row: left: station 38 @ PLUS direction; right: station 40 @ MINUS direction
3rd row: left: station 47 @ PLUS direction; right: station 43 @ MINUS direction
4th row: left: station 50 @ PLUS direction; right: station 46 @ MINUS direction

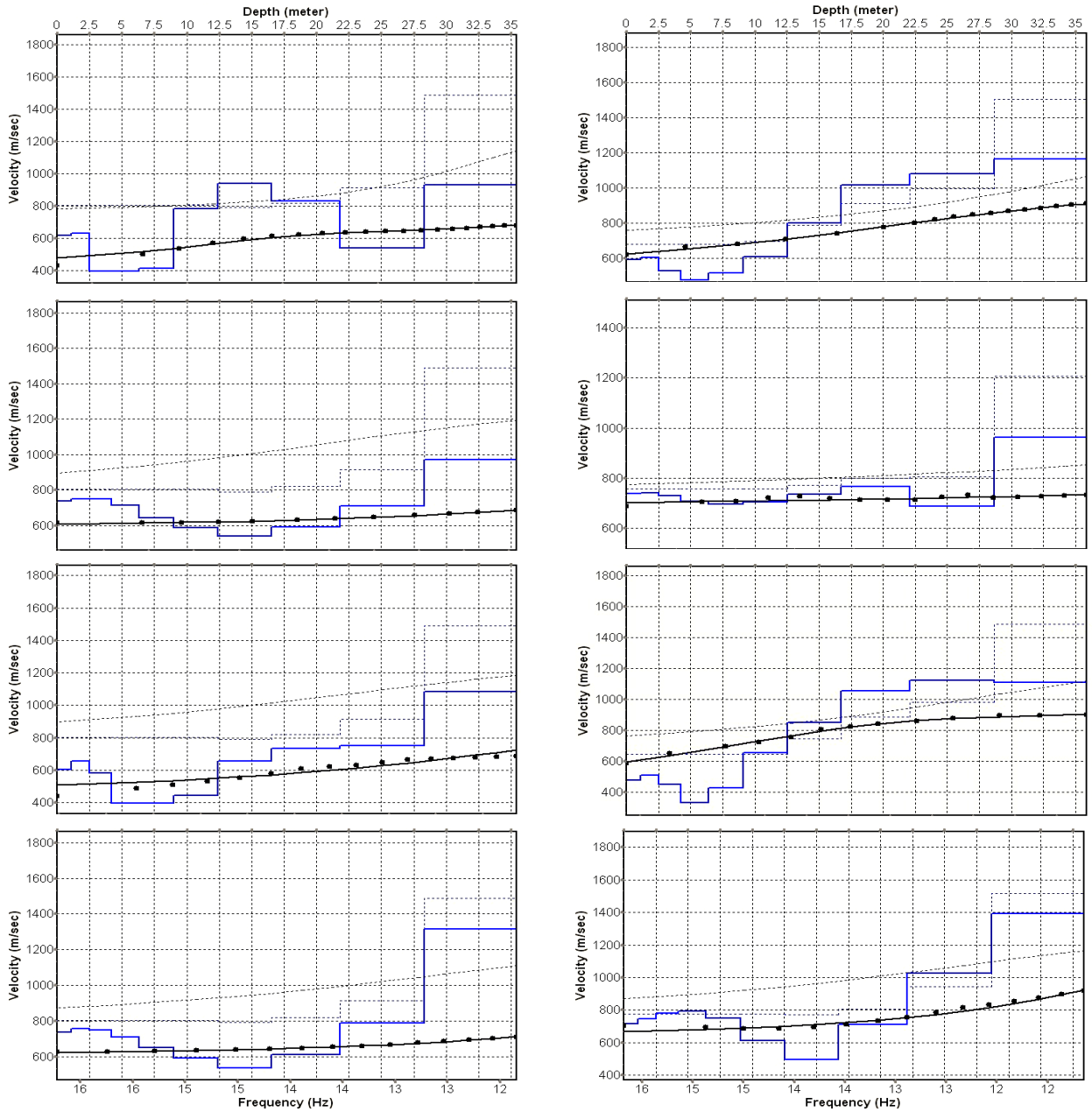

Fig. 3.3e: Inversion results of dispersion curves from dataset at line 09SN_01WEIN-M2.
***brown**: Inversion of dispersion curve (dots) resp. of the modeled dispersion curve (dotted line: initial model; continuous line: end model). Horizontal axis: frequency Hz, vertical axis: v_s.*
***blue**: 10-layer-model (dotted: initial model, continuous line: final model). Horizontal axis: depth, vertical axis: phase velocity resp. v_S).*
1st row: left: station 31 @ PLUS direction; right: station 31 @ MINUS direction
2nd row: left: station 37 @ PLUS direction; right: station 40 @ MINUS direction
3rd row: left: station 41 @ PLUS direction; right: station 46 @ MINUS direction
4th row: left: station 47 @ PLUS direction; right: station 49 @ MINUS direction

Dispersion analyses of records with longer receiver arrays should – by theory – increase the investigation depth. At WEIN, with both lines and both directions, MASW processing with the maximal array length of 96 m doesn't improve the results (Fig. 3.3f and 3.3g).

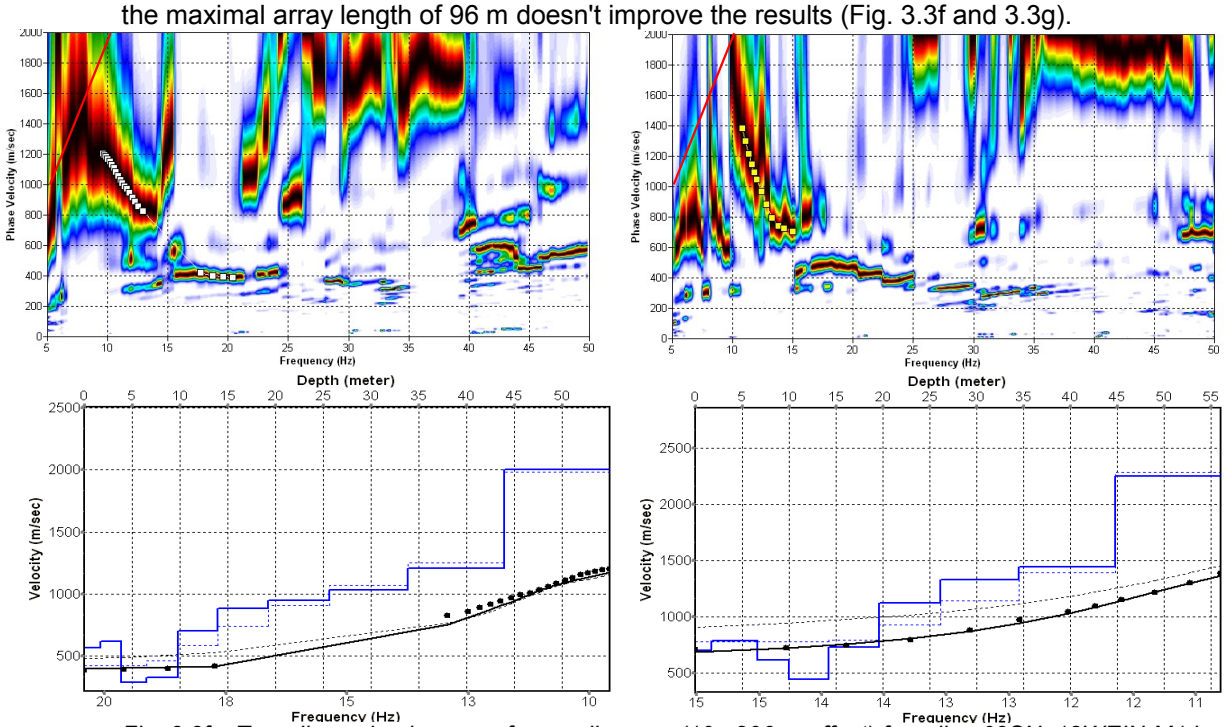

*Fig. 3.3f: Top: dispersion images of over-all arrays (10...206 m offset) from line 09SN_18WEIN-M1 in PLUS (left) and MINUS (right) direction; dotted fine line: signal-noise ratio for the designated f-v_{ph}-value. Red line: high resolution beam-forming curve for v_{max}. **Please note that the amplitudes are normalized.***
*Below: The two respective inversion results; **brown**: inversion of dispersion curve; **blue**: 10-layer-model. Horizontal axis: depth, vertical axis: phase velocity resp. v_s.*

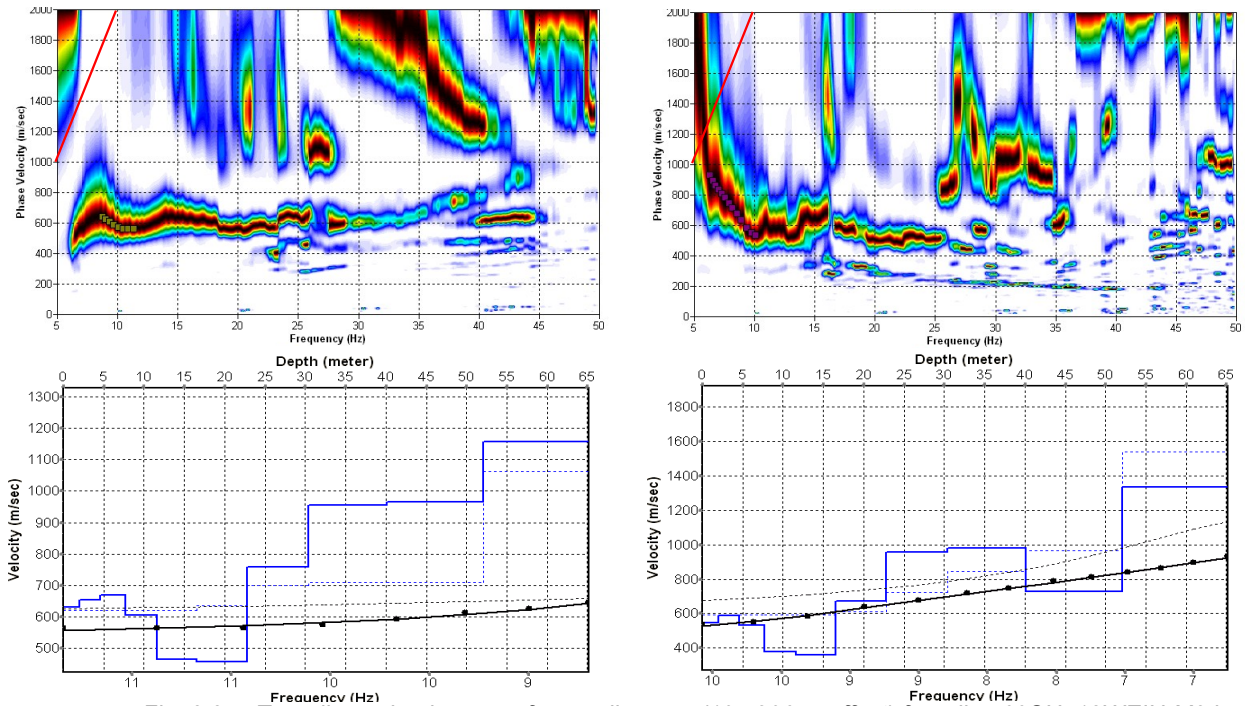

*Fig. 3.3g: Top: dispersion images of over-all arrays (10...206 m offset) from line 09SN_18WEIN-M2 in PLUS (left) and MINUS (right) direction; dotted fine line: signal-noise ratio for the designated f-v_{ph} – value. Red line: high resolution beam-forming curve for v_{max}. **Please note that the amplitudes are normalized.***
*Below: The two respective inversion results; **brown**: inversion of dispersion curve; **blue**: 10-layer-model. Horizontal axis: depth, vertical axis: phase velocity resp. v_s.*

3.3.5 Gridding and plotting of 2D v_s-velocity field

By assembling the 1D v_s - depth functions from all stations the final 2D v_s-field is derived using a Kriging gridding procedure as portrayed in Fig. 3.3h and 3.3i below:

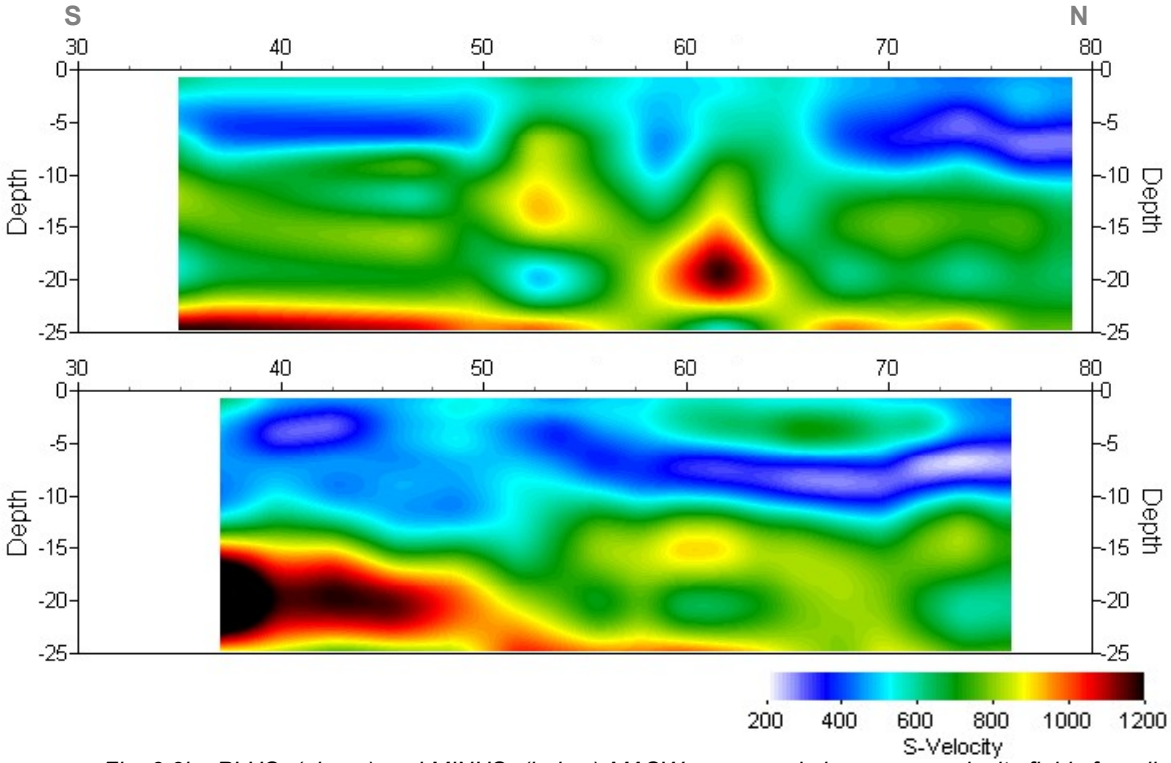

Fig. 3.3h: PLUS- (above) and MINUS- (below)-MASW-processed shear wave velocity fields from line 09SN_18WEIN-M1.

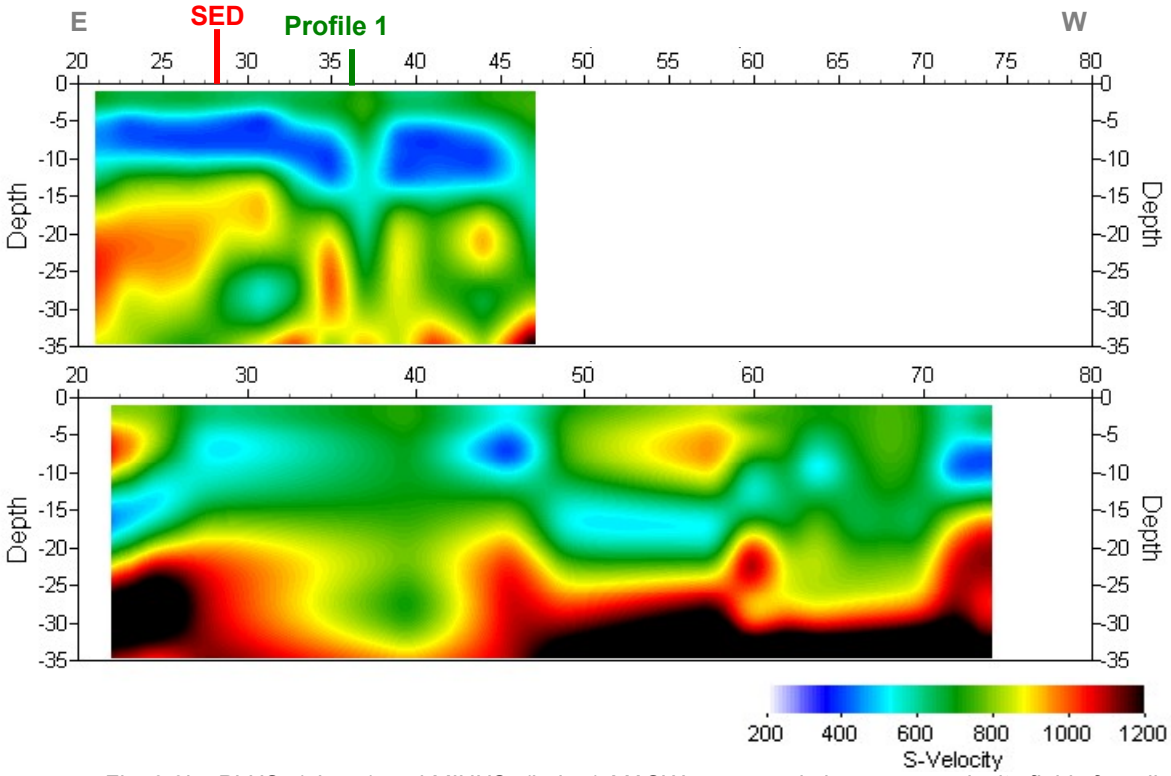

Fig. 3.3i: PLUS- (above) and MINUS- (below)-MASW-processed shear wave velocity fields from line 09SN_18WEIN-M2.

3.3.6 Calculation of the average shear wave velocity

In order to calculate a representative shear wave velocity-depth function from line 09SN_18WEIN-M1 at the SED station, all computed 1D-v_s-depth functions between seismic profile station no. 05 and 45 – that are four profiles in each direction – are averaged (non-weighted mean values). The v_s-depth-function is shown in Tab. 3.3a.

Depth [m]	Vs+ [m/s]	Vs- [m/s]	Vs [m/s]
0.8	499	576	537
1.8	519	593	556
3.0	521	588	554
4.6	485	555	520
6.5	396	508	452
8.9	397	520	459
12.0	601	648	624
15.8	820	775	797
20.5	853	705	779
25.6	883	1029	956

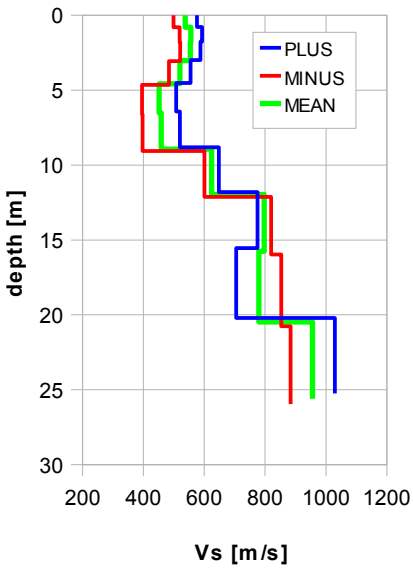

Tab. 3.3a: Averaged v_s - depth function from line 09SN_18WEIN-M1 at the SED station WEIN. Blue line: MASW-'PLUS' processing, red line: MASW-'MINUS' processing; green line: average of PLUS- and MINUS-functions.

In order to calculate an representative shear wave velocity-depth function from line 09SN_18WEIN-M2 at the SED station, all computed 1D-v_s-depth functions between seismic profile station no. 30 and 50 are averaged (non-weighted mean values). The resulting v_s-depth-function is shown in Tab. 3.3b.

Depth [m]	Vs- [m/s]	Vs+ [m/s]	Vs [m/s]
1.1	701	657	679
2.5	714	684	699
4.2	719	575	647
6.4	686	467	576
9.1	646	455	550
12.4	635	590	612
16.7	702	766	734
21.9	907	857	882
28.5	1045	798	921
35.6	1437	900	1169

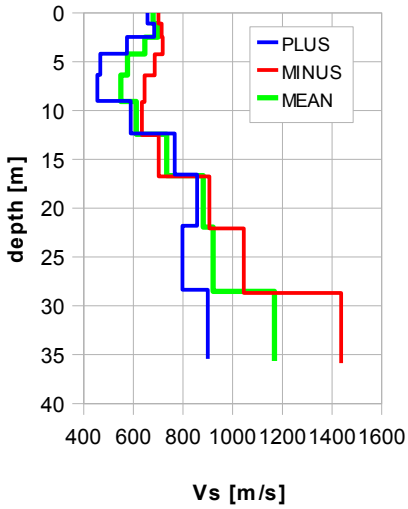

Tab. 3.3b: Averaged v_s - depth function from line 09SN_18WEIN-M2 at the SED station WEIN. Blue line: MASW-'PLUS' processing, red line: MASW-'MINUS' processing; green line: average of PLUS- and MINUS-functions.

The inversion of the four 100 m-array dispersion curves data (10 to 106 m offset, see Fig. 3.3f and 3.3g) are given in Tab. 3.3c. These values are complemented with the values derived from the 40 m-arrays analyses (Tab. 3.3a and 3.3b).

100 m array								40 m array			
depth	m1+	m1-	m2+	m2-	m1	m2	m	depth	m1	depth	m2
1.9	569	699	631	548	634	589	633	0.8	576	1.1	499
4.2	622	789	653	588	705	620	688	1.8	593	2.5	519
7.1	292	790	670	531	541	600	584	3.0	588	4.2	521
10.8	329	618	605	377	474	491	518	4.6	555	6.4	485
15.4	701	443	465	362	572	413	536	6.5	508	9.1	396
21.1	882	730	456	672	806	564	689	8.9	520	12.4	397
28.2	948	1121	758	955	1035	857	942	12.0	648	16.7	601
37.1	1034	1331	955	980	1182	967	1106	15.8	775	21.9	820
48.3	1210	1444	966	728	1327	847	1207	20.5	705	28.5	853
60.3	2004	2249	1157	1336	2127	1246	1803	25.6	1029	35.6	883

Tab. 3.3c: v_s-depth values from the four MASW-derived dispersion curves of both seismic line 09SN_18WEIN-M1 and 09SN_18WEIN-M2 using 100 m-arrays. The dispersion curves are shown in Fig. 3.3f and Fig 3.3g).

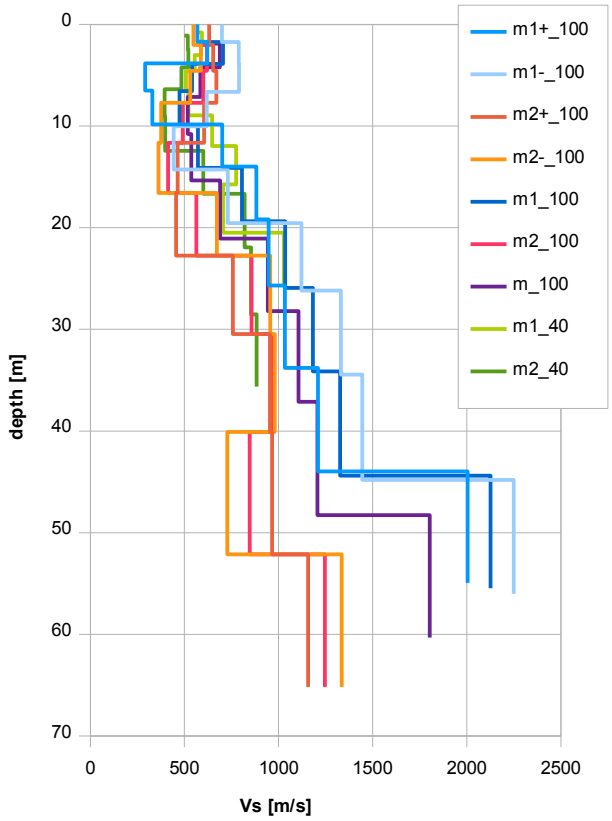

Fig. 3.3j: Comparison of the ensemble of inversion results of both lines 09SN_18WEIN-M1 and -M2, either using the 40 m- and the 100 m-arrays.
blue lines: analyses of records from line 09SN_18WEIN-M1
red lines: analyses of records from line 09SN_18WEIN-M2
violet line: mean of both 100 m-array records analyses in MINUS and PLUS direction.
green lines: v_s-values from analyses of 40 m-array records.

3.3.7 Calculation of the shear wave velocity scalars $v_{s,5}$, $v_{s,10}$, ...

The parameters $v_{s,5}$, $v_{s,10}$, $v_{s,20}$, $v_{s,30}$, $v_{s,40}$, $v_{s,50}$ represent the average shear wave velocities in the depth interval between the surface and the respective depth levels and are determined from the formula

$$v_{s,n} = \frac{\sum_{i=1}^{n} d_i}{\sum_{i=1}^{n} d_i / v_{si}}$$

with:

d_i = thickness of layer i

v_{si} = corresponding shear-wave velocity.

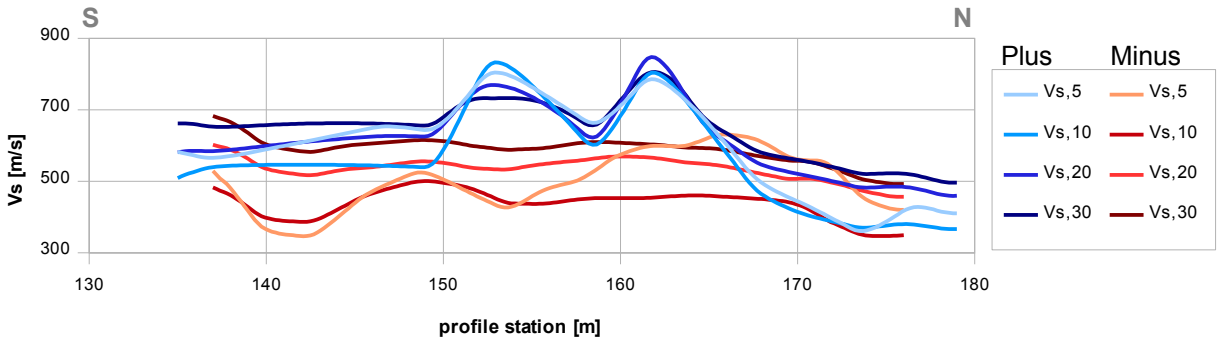

Fig. 3.3k: Graphs of the averaged $v_{s,5}$...-values along the line 09SN_18WEIN-M1 for the PLUS- (blue lines) and MINUS- (red lines) directions.

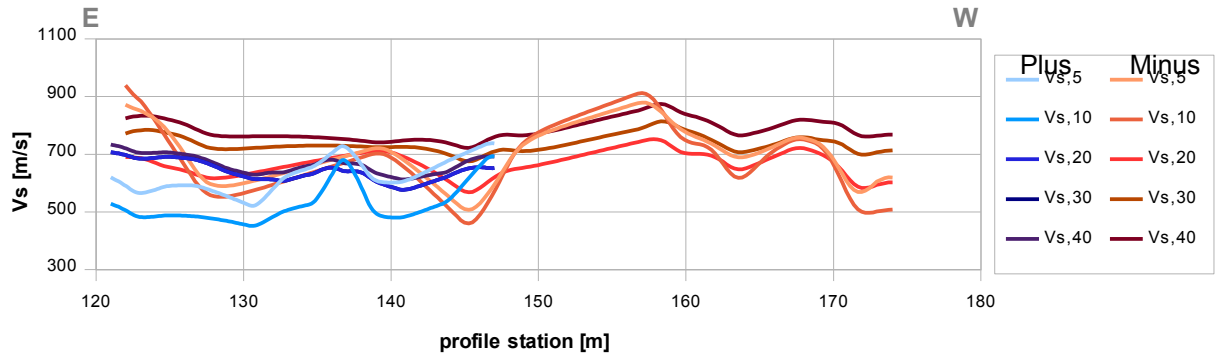

Fig. 3.3l: Graphs of the averaged $v_{s,5}$...-values along the line 09SN_18WEIN-M2 for the PLUS- (blue lines) and MINUS- (red lines) directions.

The average values of the s-wave velocity model $v_{s,5}$, $v_{s,10}$, $v_{s,20}$, $v_{s,30}$, $v_{s,40}$, $v_{s,50}$, $v_{s,100}$ (= average shear wave velocity from the surface to depths of 5 m, …until 100 m) on the line segment nearest to the SED station (Tab. 3.3d) are summarized below:

	Vs,5	Vs,10	Vs,20	Vs,30	Vs,40	Vs,50
MINUS	400	419	539	608	n/a	n/a
PLUS	599	542	602	659	n/a	n/a
MEAN	500	480	571	633	n/a	n/a

	Vs,5	Vs,10	Vs,20	Vs,30	Vs,40	Vs,50
MINUS	651	628	656	718	754	n/a
PLUS	645	545	622	622	649	n/a
MEAN	648	586	639	670	702	n/a

Tab. 3.3d: The average shear wave velocities within the depth intervals from surface down to 5 m, etc.… to 50 m, calculated for the line segment with a subjectively most similar geology to the SED station (profile station 05 to 45 for line 09SN_WEIN-M1, above; profile stations 30 to 50 for line 09SN_18WEIN-M2, below).

3.4 Hybrid Seismic Data Processing

3.4.1 p-wave *Reflection* Seismic Processing Sequence

A) Data conditioning

A1 Reformatting and quality verification of field data
A2 Recording geometry assignment
A3 Data editing (suppression of bad / dead traces, etc.)
A4 Preliminary analysis of refraction velocities

B Filtering and deconvolution

B1 Analytical muting of refraction arrivals
B2 Amplitude recovery / amplitude equalization in time and frequency domains
B3 Predictive deconvolution parameter tests / application
B4 Determination of band limiting corner frequencies / application
B5 Optional 2-D filtering

C) Velocity analysis and stack

C1 Common Depth Point (CDP) sort
C2 Semblance velocity analysis using supergathers of 3 - 5 CDP's
C3 Optional dip move-out correction
C4 Normal Move-Out (NMO) correction and application of stretch mute
C5 Band-pass filtering
C6 CDP stack
C7 Optional coherency filtering

D) Time-depth conversion

D1 Optional spiking deconvolution
D2 Band-pass filtering
D3 Depth conversion
D4 Final display of seismic depth section with inversed polarity (non-SEG-convention)

3.4.2 The presentation of reflection seismic data

The data in a reflection seismic section are presented as an assembly of individual seismic signals at regular intervals along a seismic profile. The simplest way of representing the signals are single wiggle lines (first to the left in the illustration below). A more capturing presentation is the variable area form (second to the left). Combining these two modes results in the var-wiggle mode. Another method of data visualization is the variable density mode (second from the right).

The compressional phase of seismic signals is defined in this report as the onset of the positive amplitude excursion in black (Fig. 3.4a). Since the source signal is produced by an explosion or by an impact at the surface, the signal starts off with a compression of the ground particles. Thus the arrivals of reflection events are defined by the compressional phase.

In rare situations of velocity inversions, cases in which formation velocities are lower than in the layers above, polarity reversals of the reflected signals occur. The beginning of the reflection event would then be characterized by a dilatational phase, represented in this report as a negative amplitude excursion, i.e. in white.

The final p-wave seismic depth sections are displayed in Fig. 3.4b and 3.4c, the hybrid sections in Fig. 3.4j and -k further below.

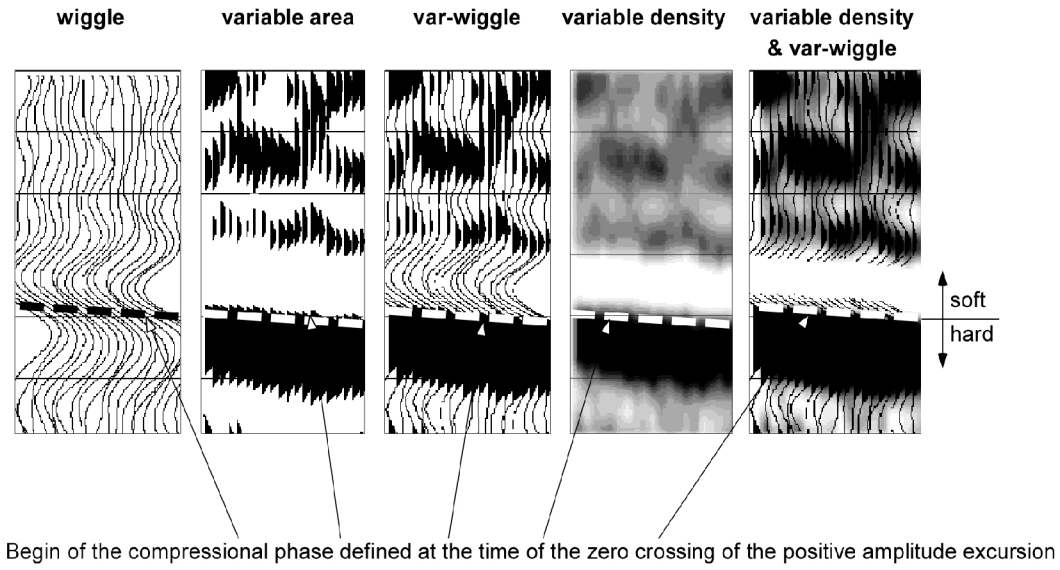

Fig. 3.4a Representation of reflection seismic data and the definition of a reflection event.

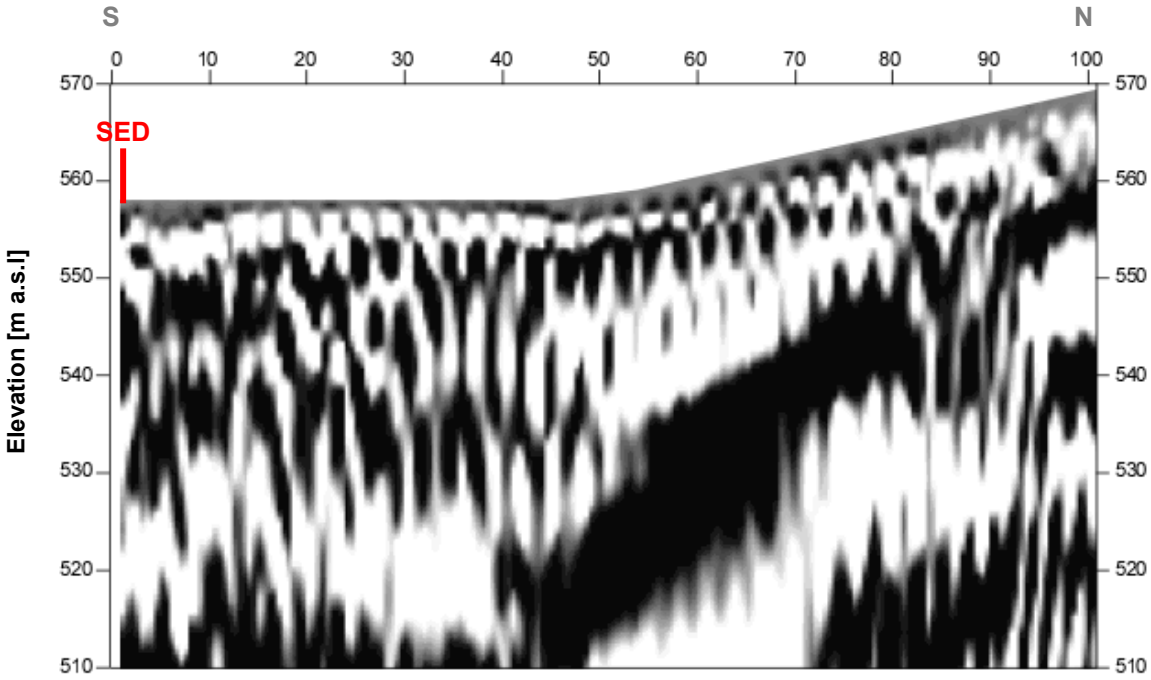

Fig. 3.4b: Seismic depth section of seismic line 09SN_18WEIN-P1 with variable density mode presentation. Vertical axis: elevation [m a.s.l.], horizontal axis: profile meter; no vertical exaggeration. The station spacing is 1 m.

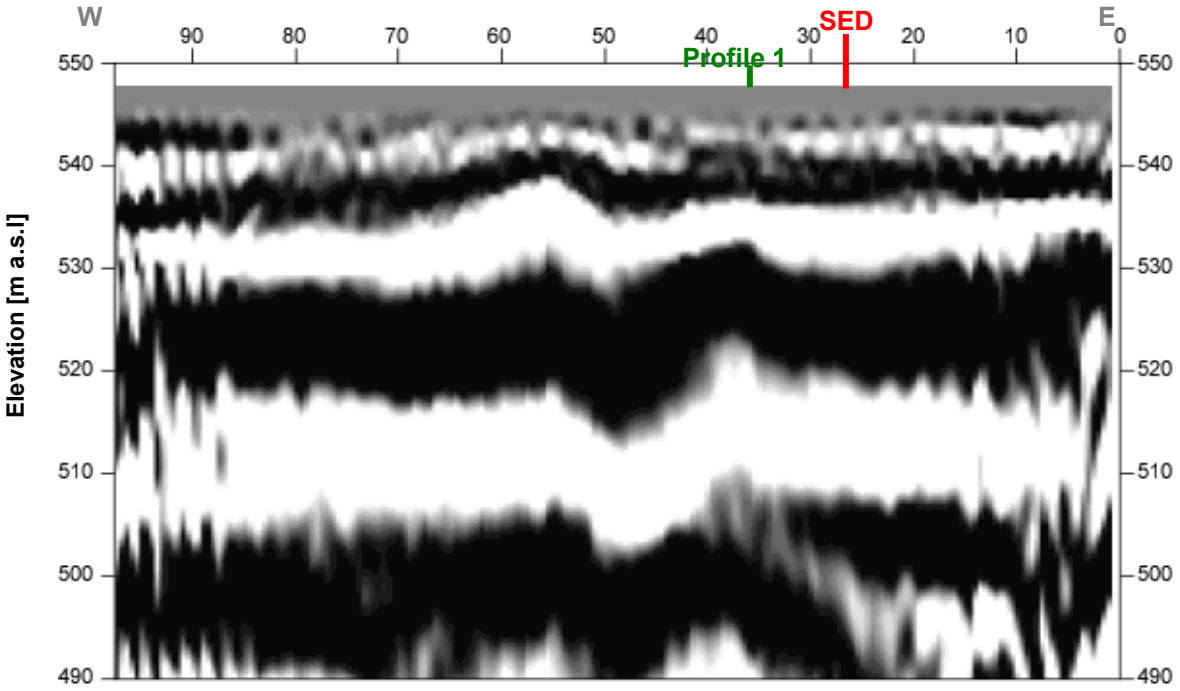

Fig. 3.4c: Seismic depth section of seismic line 09SN_18WEIN-P1 with variable density mode presentation. Vertical axis: elevation [m a.s.l.], horizontal axis: profile meter; no vertical exaggeration. The station spacing is 1 m.

3.4.3 p-wave refraction tomography processing

The seismic p-wave refraction processing steps are analogous to those described in paragraph 3.2. For a detailed method statement and a description of the processing steps please refer to the summary report. The Figs. 3.4d to 3.4i and Tab. 3.4a illustrate the intermediate processing steps and the final result.

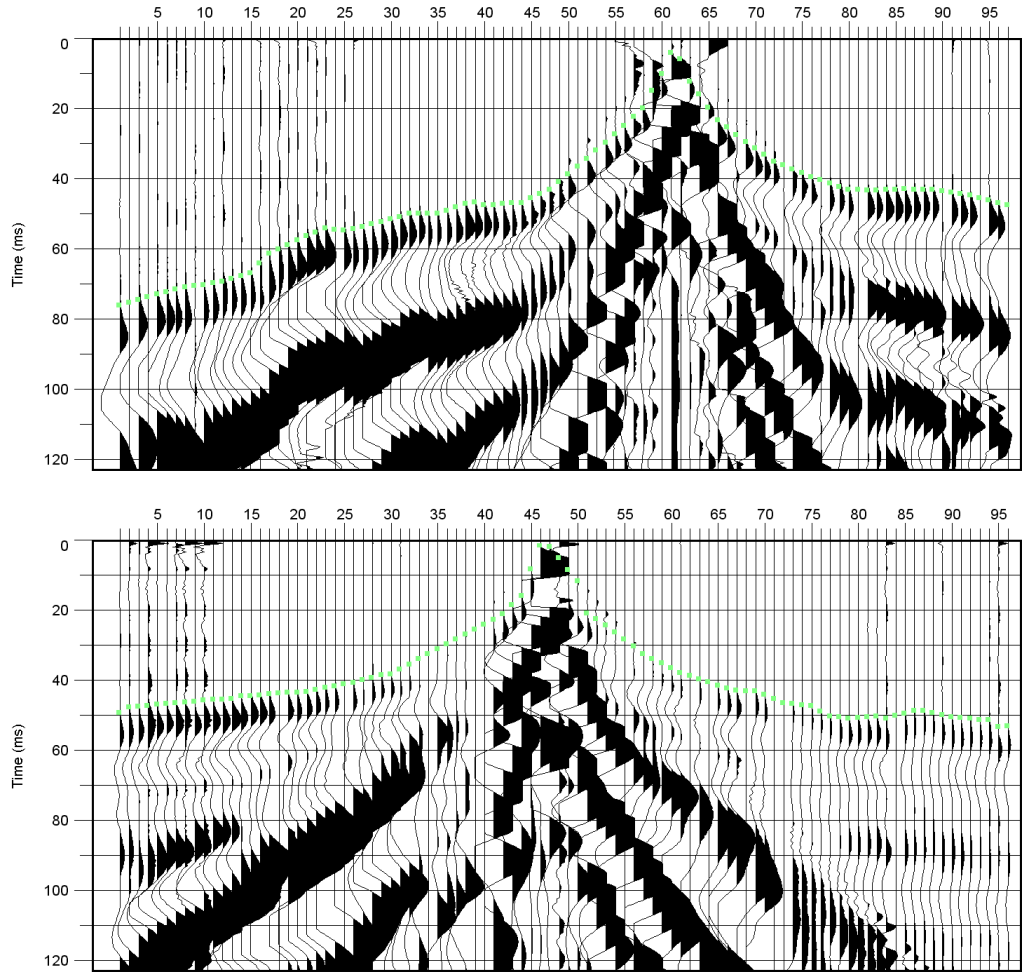

Fig. 3.4d: p-wave records from 09SN_18WEIN-P1 (above) and -P2 (below) with positive amplitude excursions in black. Blue dots mark the manually picked first break arrival times. Vertical axis: travel time in ms, horizontal axis: station numbers spaced at 1 m.

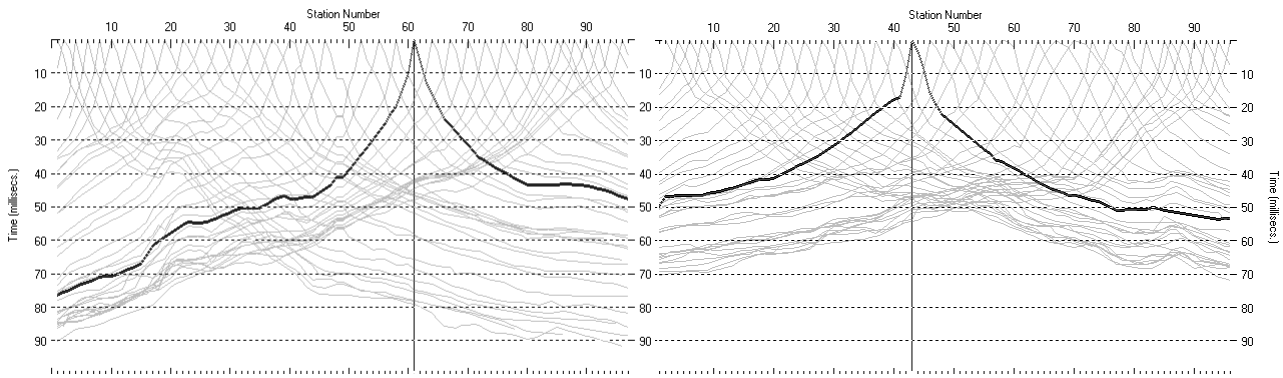

Fig. 3.4e: Travel time curves of p-wave arrival time picks from line 09SN_18WEIN-P1 (left) and -P2 (right). Vertical axes: travel time [ms], horizontal axes: station number (= profile meter).

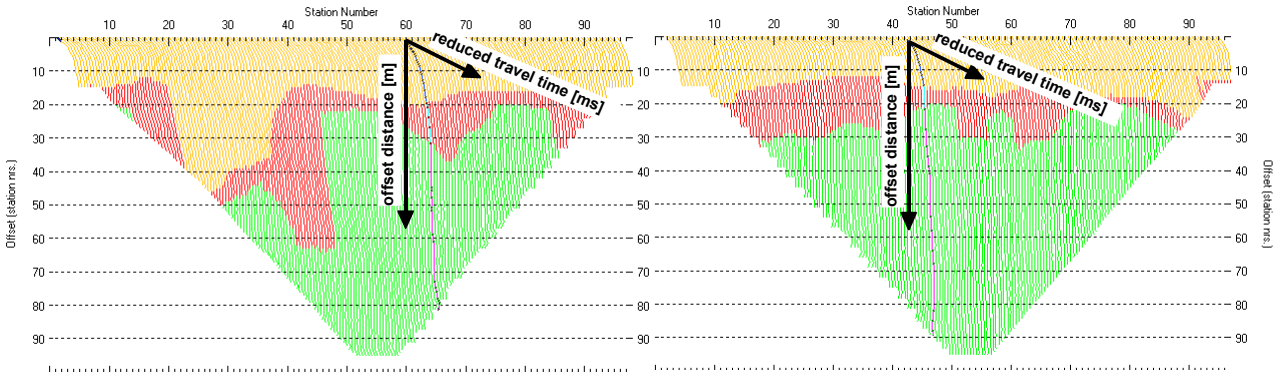

Fig. 3.4f: 3-dimensional distance-travel time diagrams at the mid-points between source points and receiver stations are instrumental when using the analytical CMP derivation of the initial velocity field. The horizontal axes are along the CMP positions and the travel time respectively, the vertical axis denotes the offset distance between source and receiver positions.

Depth [m]	Vp [m/s]
0.2	244
0.5	291
0.9	338
1.4	412
2.1	498
2.9	599
4.1	747
5.7	857
7.6	1053
10.2	1378
13.6	1854
18.1	2029
24.0	2433
31.5	3530
41.5	5260

Depth [m]	Vp [m/s]
0.0	190
0.2	194
0.5	228
1.0	294
1.7	429
2.5	593
3.7	752
5.2	902
7.3	1203
10.2	1694
14.0	2137
19.3	2502
26.5	3001
36.3	3989
49.6	4966

Tab. 3.4a: Initial 1D p-wave velocity model derived from real data (left: 09SN_18WEIN-P1; right: -P2).

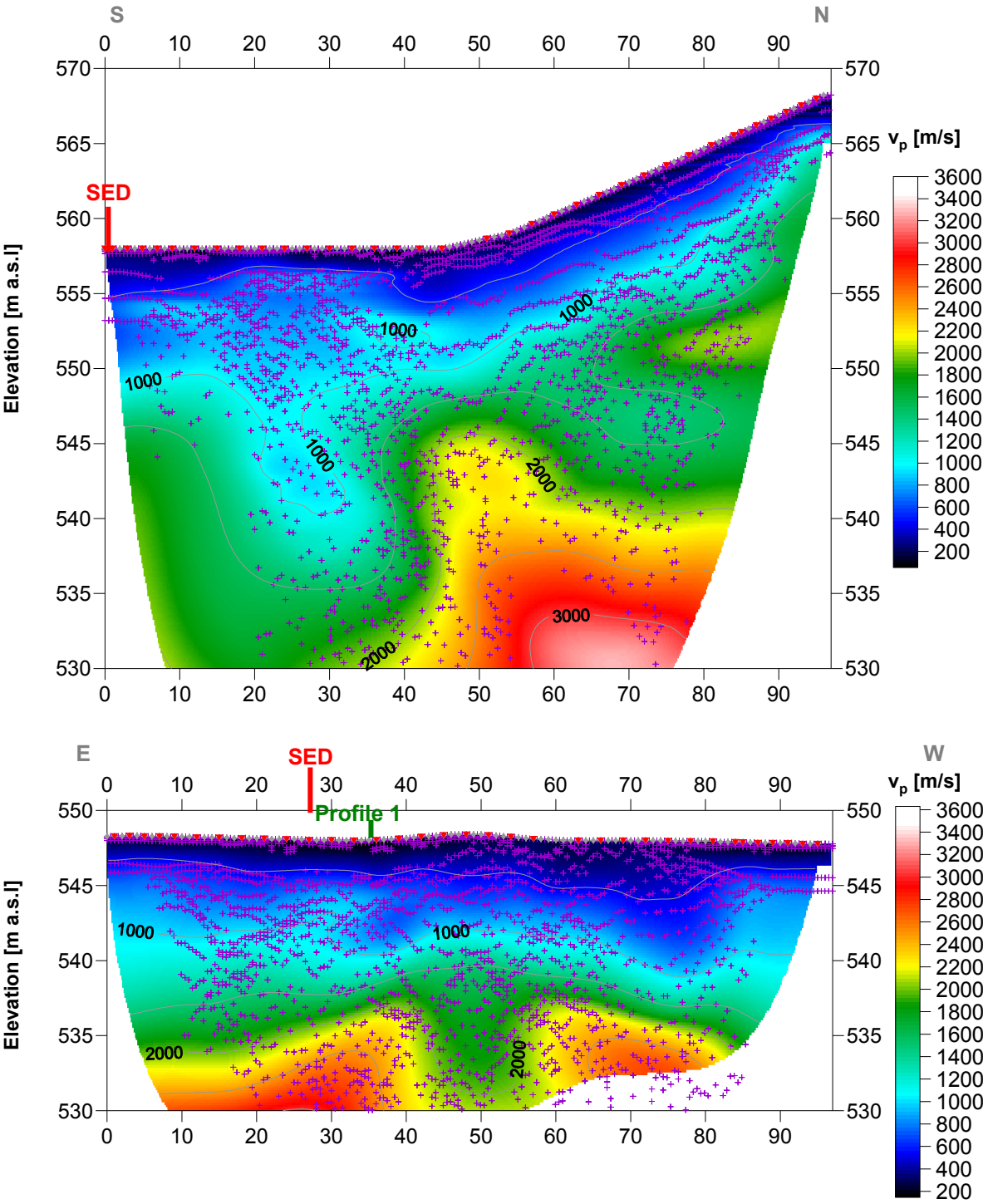

Fig. 3.4g: Compressional wave velocity field image along the seismic profiles 09SN-18WEIN-P1 (above) and -P2 (below). Red/white colors indicate solid rock, blue/black colors unconsolidated sediments and soil. Vertical axis: elevation [m a.s.l]; horizontal axis: profile meter; color scale: v_s [m/s]; vertical exaggeration: 2:1; gray squares: receiver stations; red triangles: shot positions; magenta crosses: positions of determined velocity values.

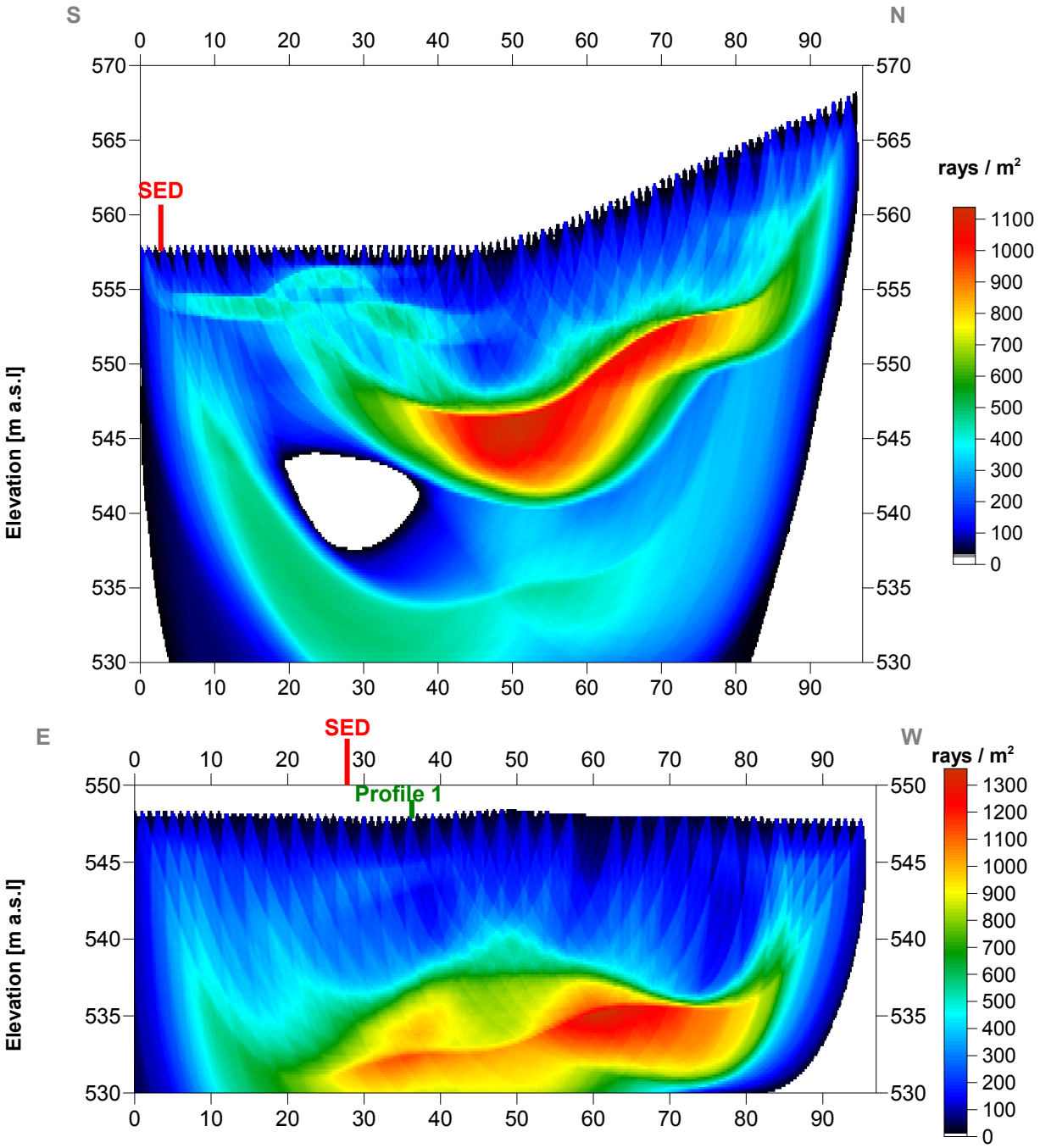

Fig. 3.4h Compressional wave subsurface ray path density along the seismic profiles 09SN_18WEIN-P1 (above) and -P2 (below). Red/white colors indicate high velocity contrast between two layers, blue/black colors low coverage areas. Vertical axis: elevation [m a.s.l]; horizontal axis: profile meter; color scale: ray paths per m²; vertical exaggeration: 2:1.

Depth [m]	Vp [m/s]
0.0	132
2.2	576
4.3	825
6.4	872
8.4	976
10.5	1189
12.6	1357
14.6	1397
16.7	1414
18.8	1473
20.9	1555
22.9	1659
25.0	1782
27.1	1896
29.1	2010
31.2	2119
33.3	2231
35.3	2357
37.4	2555
39.5	2747
41.5	2896

Depth [m]	Vp [m/s]
0.0	184
1.0	286
2.0	450
3.0	627
4.0	772
5.0	823
6.0	883
7.0	1013
8.0	1199
9.0	1403
10.0	1600
11.0	1792
12.0	1974
13.0	2098
14.0	2183
15.0	2246
16.0	2297
17.0	2349
18.0	2404
19.0	2451
20.0	2985

Tab. 3.4b: Final 1D p-wave velocity model derived from real data at positions most similar to the geological setting at SED station between profile meters 05 and 45 at line 09SN_18WEIN-P1 (left) resp. 30 and 50 at line 09SN_18WEIN-P2 (right) .

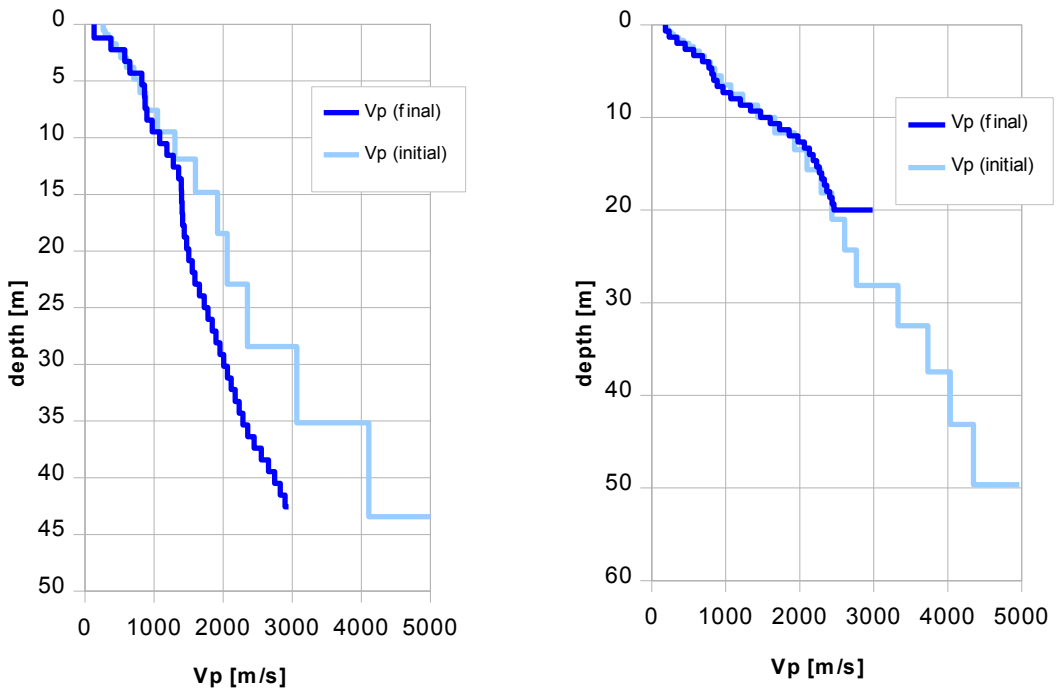

Fig. 3.4i: Final 1D p-wave velocity model derived from real data at a position most similar to the geological setting at the SED station between profile meters 05 and 45 at line 09SN_18WEIN-P1 (left) resp. 30 and 50 at line 09SN_18WEIN-P2 (right). Initial 1D p-wave velocity model values are given in Tab. 3.4a.

3.4.4 Representation of the hybrid seismic section

The hybrid seismic section is the reflection seismic section with the superimposed p-wave velocity field. It portrays the geological structures and the p-wave velocity field, the latter being indicative for the rock / soil rigidity. The uninterpreted hybrid seismic section is portrayed in Fig. 3.4j and 3.4k below.

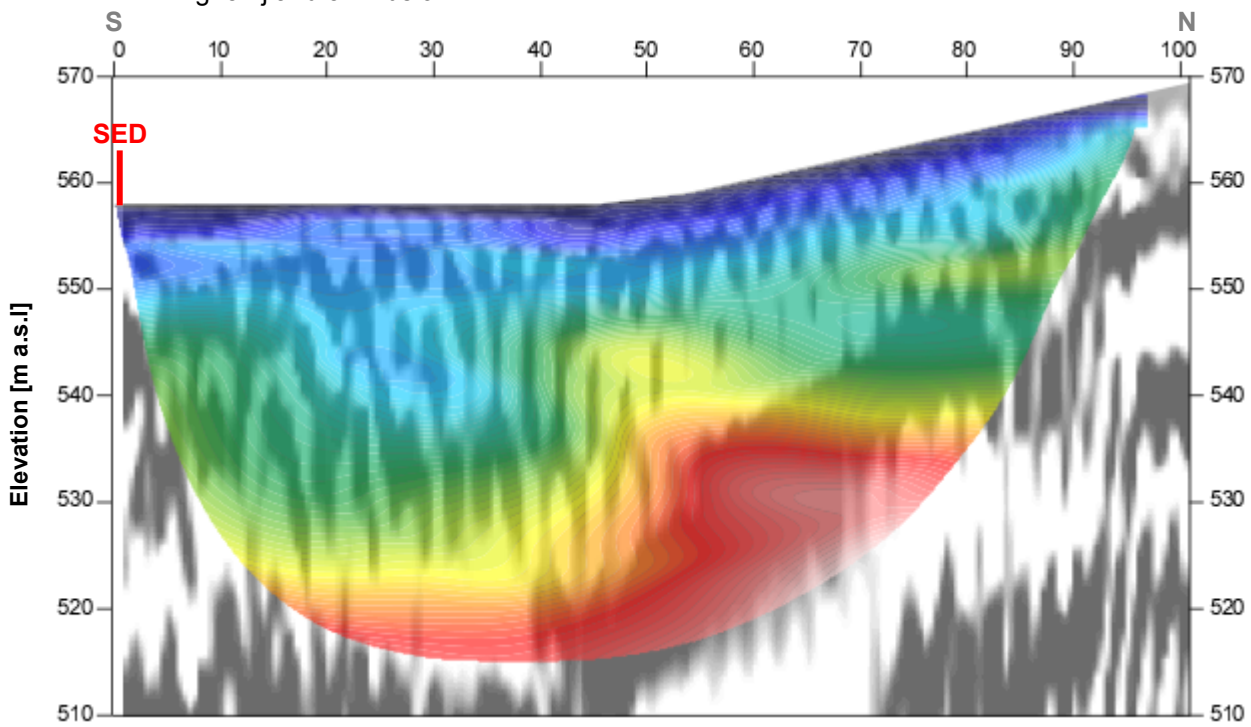

Fig. 3.4j Uninterpreted hybrid seismic section 09SN_18WEIN-P1: superimposed onto the seismic reflection section is the color encoded p-velocity field derived by refraction tomography (no vertical exaggeration).

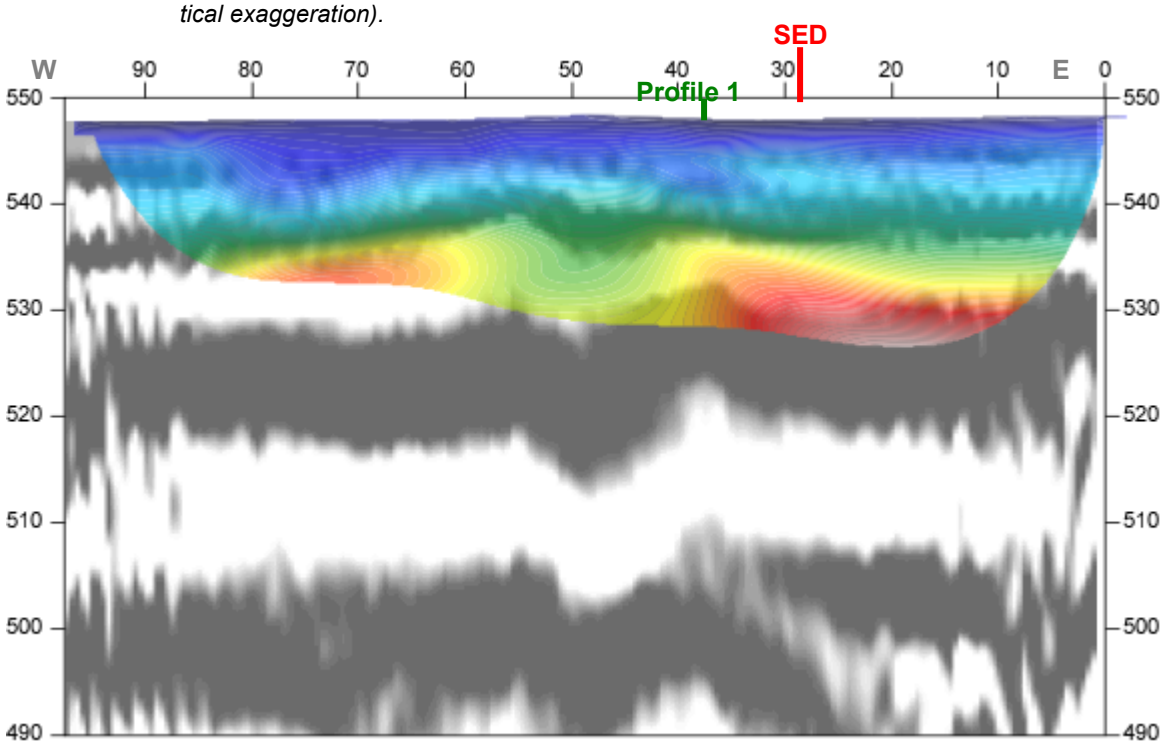

Fig. 3.4k Uninterpreted hybrid seismic section 09SN_18WEIN-P2: superimposed onto the seismic reflection section is the color encoded p-velocity field derived by refraction tomography (no vertical exaggeration).

4 DISCUSSION OF THE RESULTS

4.1 Summary and Validation of the Results

Compressional and shear wave velocity data from refraction seismic surveys both p-wave and s-wave and also the MASW survey data from profile 09SN_18WEIN-1 are shown in Tab. 4.1 for the uppermost 40 m. The theoretical shear wave velocity $v_{s(calc)}$ in Tab. 4.1 is calculated by using a theoretical v_p/v_s-ratio of $\sqrt{3}$.

Depth	Vp1	Vp2	Vs1	Vs2	Vs1	Vs2	Vs1	Vs2
	meas	meas	calc	calc	meas	meas	MASW	MASW
0	132	184	76	106	139	117		
1	378	235	218	136		134	537	701
2	576	450	333	260	246	230	556	714
3	651	567	376	328	355	308	554	
4	825	772	476	445		386		719
5	862	811	498	468	395	516	520	
6	872	883	504	510		379		686
7	897	962	518	555	392	390	452	
8	976	1199	563	692	415	408		
9	1083	1335	625	771		448	459	646
10		1600		924	459			
11	1189	1728	687	998				
12	1281	1974	739	1140	483		624	635
13	1357	2063	784	1191	495			
14	1395	2183	805	1260				
15	1397	2227	807	1286	517			
16	1407	2297	813	1326	567		797	702
17	1414	2331	816	1346				
18	1440	2404	831	1388	609			
19	1473	2438	850	1407				
20	1505	2985	869	1723	649			
21	1555		897		689		779	
22	1594		920					907
23	1659		958		762			
24	1726		996					
25	1782		1029		837			
26	1842		1063		923		956	
27	1896		1095					
28	1954		1128		1039			1045
29	2010		1160					
30	2063		1191		1164			
31	2119		1223					
32	2176		1256					
33	2231		1288					
34	2287		1321					
35	2357		1361					
36	2450		1415					1437
37	2555		1475					
38	2658		1534					
39	2747		1586					
40	2828		1633					

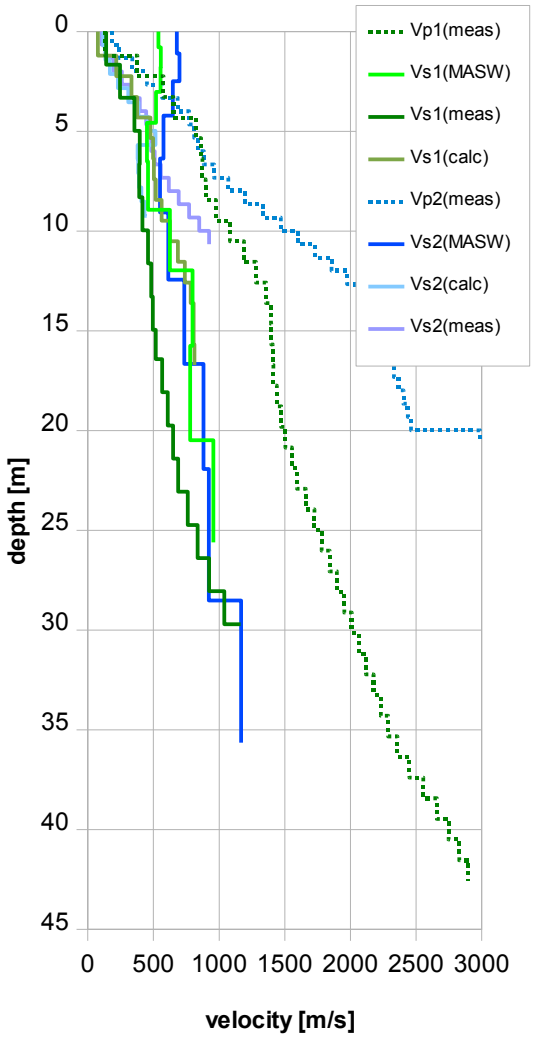

Tab. 4.1: Shear and compressional wave velocity model determined at the SED station WEIN.

Fig. 4.1: Graphic display of shear (continuous lines) and compressional (dotted lines) wave velocities determined at the SED station. In green colors values from line 09SN_18WEIN-1 and in blue values from line 09SN_18WEIN-2. at the SED station.

4.2 Validation of the methods and their results

Due to methodological differences, v_s velocities derived by MASW analysis and by the refraction tomography technique may differ considerably. This is because MASW analysis cannot image small rock/soil inhomogeneities as a dispersion image with an array length of i.e. 40-m only yields one single v_s-value at each depth. On the other hand, refraction diving wave tomography results produce v_s-sections with a high lateral resolution, but fail to provide information at greater depths.

4.3 Error Estimates

The error estimates given in Tab. 4.3 below are relevant only in the context of this survey.

Surveying method	Type of result	Error estimate
v_s – refraction tomography	v_s – velocity field image	10%
MASW only "+" or only "-" values*	v_s – velocity field image	15%
MASW (mean of "+" & "-" values)*	v_s – velocity field image	10%
v_p – refraction tomography	v_p – velocity field image	8%
Reflection seismic surveying	Image of subsurface structures	n.a.

** MASW values in the uppermost 7 m are prone to an error of about 30 % (only one direction) resp. 20 % (mean of both directions.*

Tab. 4.3 Error estimates for the methods applied. Note that higher error estimates are to be taken into account with increasing depths.

The above error estimates are of a qualitative character only. In view of the intense fluctuations to be expected in both the lateral and vertical directions, any attempt to derive a quantitative general error estimate to be valid for the entire survey is to be considered as futile. In particular the topography variations on line 09SN_18WEIN-1 have a certain impact on the quality of dispersion images. Nevertheless, all velocity data coincide well, independently from the methodological differences.

At the SED station WEIN (Weingarten TG), the refraction velocity images both from shear and compressional wave analysis show coincident structures. The MASW figures are in the same range as the values obtained from the shear wave diving wave refraction tomography surveys.

4.4 The Geophysical Interpretation

The most conclusive information about the subsurface structures is provided by the results of the hybrid seismic section (v_p-refraction tomography profiling and reflection seismic section) and confirmed by the evaluation results of the v_s-refraction tomography data.

As can be seen from the v_s and v_p refraction tomography sections in Fig. 3.2e/f & Fig. 3.4g/h, the topography of the bedrock surface is imaged in detail on both profiles. In the most northern 30 m (profile meter 70 to 100, the bedrock depth seems to be less than 10 m. To the south, the bedrock surface is situated at a depth of about 30 m.

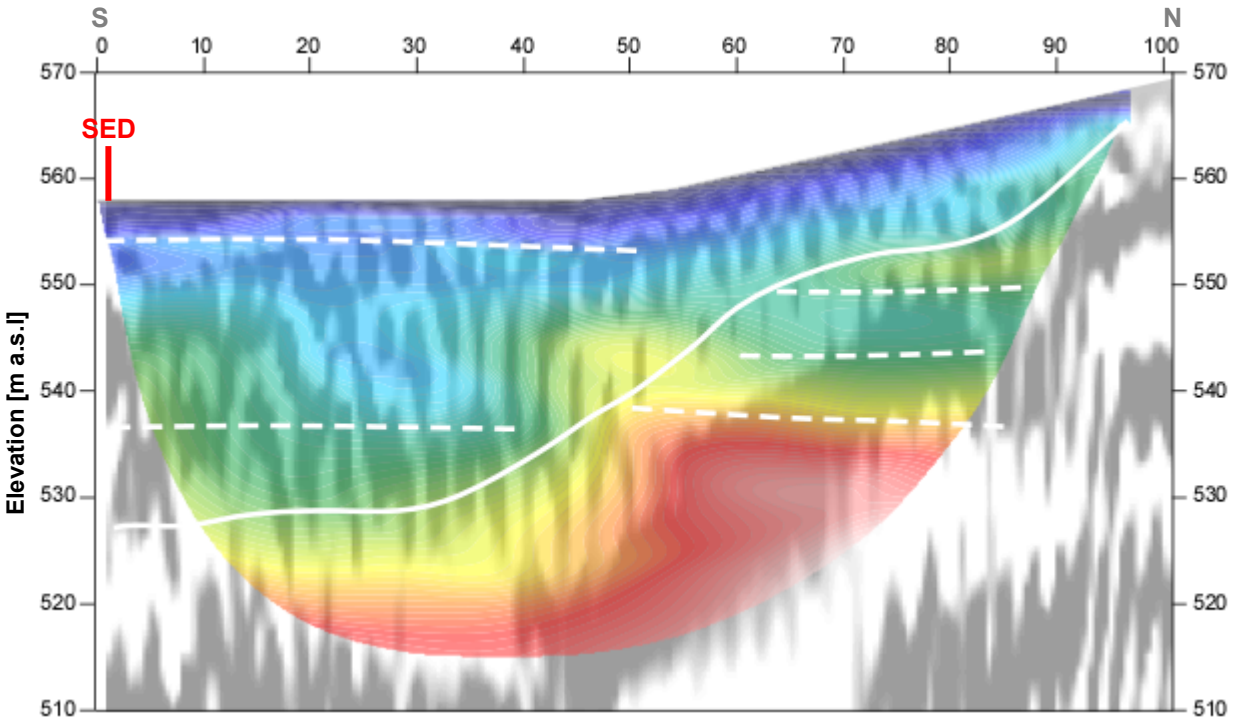

Fig. 4.2a Geophysical interpretation of the hybrid seismic section 09SN_18WEIN-P1. White lines denote layer boundaries, continuous line the bedrock surface.

Also on the second hybrid section 09SN_18WEIN-2, the topography of the bedrock surface is imaged in detail all over the profile. Approximate in the middle of the profile, a potential tectonic (?) loosening zone in the bedrock is clearly visible, both in refraction and reflection seismic sections. This zone is possibly in line with the deep reaching bedrock surface in profile 09SN_18WEIN-1.

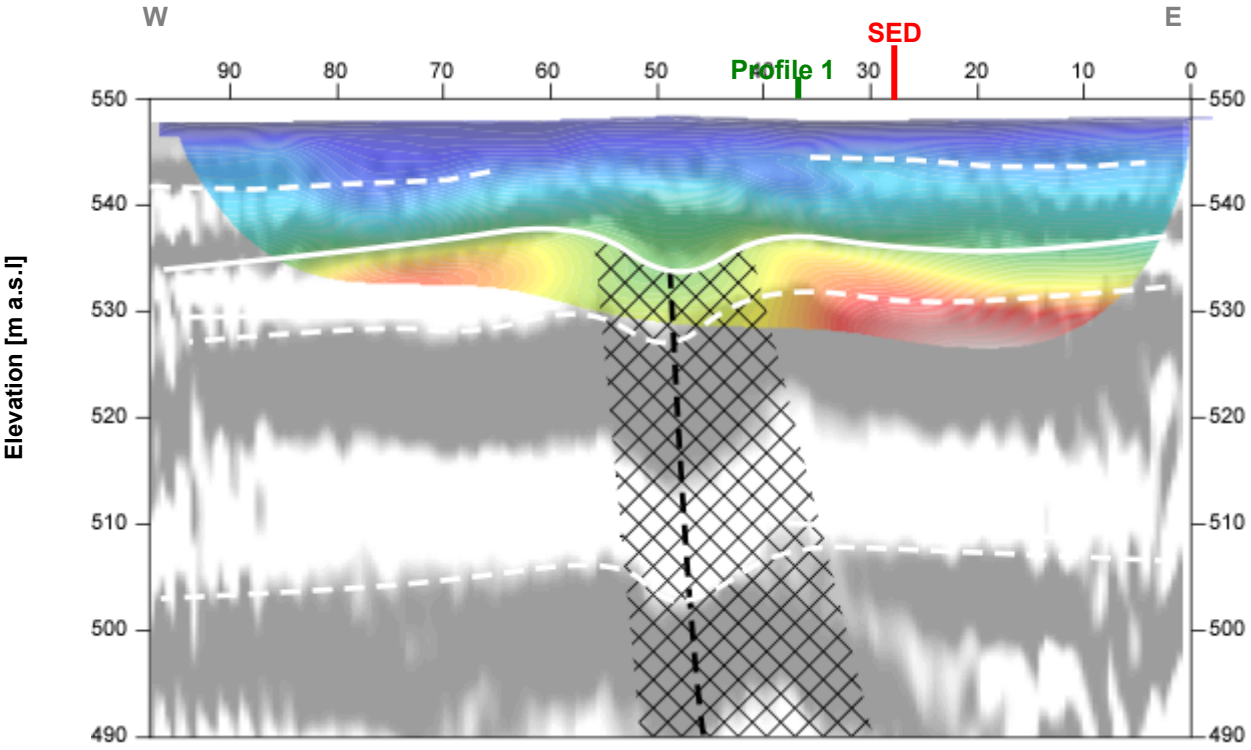

Fig. 4.2b Geophysical interpretation of the hybrid seismic section 09SN_18WEIN-P2. White lines denote layer boundaries, the continuous one marks the bedrock surface; black dotted lines are indicative of suspected faulting with a wide loosening zone (black hatched area).

5 SUMMARY AND CONCLUSIONS

- In March 2009 a combined seismic s- and p-wave survey was carried out at the SED earthquake monitoring station near Weingarten TG.
- The shear wave data have been evaluated by conventional diving wave refraction tomography techniques in order to derive the s-wave velocity field along the seismic line. Due to the inherent constraints of the refraction tomography method, the depth of investigation is limited to 8 to 20 m under the prevailing geological conditions.
- The p-wave data have been processed
  - firstly to derive a 2D s-wave velocity field by using the MASW (**M**ultichannel **A**nalysis of **S**urface **W**aves) technique;
  - and secondly, according to the hybrid seismic data processing scheme for representing the subsurface structures in a combined reflection seismic section with the superimposed p-wave velocity field.
- The shear wave velocity range determined by the MASW method in the uppermost 30 meters spans from values of 537 m/s to 1437 m/s.
- The scalar values derived by the MASW survey at the SED station (seismic line 09SN_18-WEIN-M1, profile station 35; seismic line 09SN_18WEIN-M2, profile station 40) are the following:

line 1			line 2		
$v_{s,5}$	=	500 m/s	$v_{s,5}$	=	648 m/s
$v_{s,10}$	=	480 m/s	$v_{s,10}$	=	586 m/s
$v_{s,20}$	=	571 m/s	$v_{s,20}$	=	639 m/s
$v_{s,30}$	=	633 m/s	$v_{s,30}$	=	670 m/s
$v_{s,40}$	=	n/a	$v_{s,40}$	=	702 m/s

- The maximum refraction shear wave velocity derived is 1164 m/s at a depth of 29.7 m.
- The maximum p- wave velocity determined is 2985 m/s at a depth of 40 m.
- The geophysical interpretation of the subsurface structures in this report are to be validated and incorporated into a comprehensive appraisal by a geologist familiar with the local geological setting.

Schwerzenbach, 4th May 2009

Walter Frei
dipl. Natw. ETH
managing director

Lorenz Keller
dipl. Natw. ETH
project manager